CalVal Support System

In response to

ESA – Request for Quotation RFQ/3-11336/05/I-OL
“INTER-COMPARISON DATA, PROTOCOLS & GUIDE LINES DEFINITION FOR CAL &VAL”,
dated Frascati, 10. May 2005
Statement of Work
GMES-CLVL-EOPG-SW-05-0001

Calibration Requirements Consolidation

Deliverable D1-3

Annexes

Deliverables Summary Sheet

Project number		
Project acronym		
Project title	CalVal Support System	
Deliverable No.	D1-3	
Short description	Calibration Requirements Consolidation	
Version	1.2	
Author(s) and affiliation(s)	R. Santer for Brockman Consultant	
Modification history	2005-08-23:	Preliminary draft
	2005-12-22:	First delivery to ESA
	2006-06-22	Consolidated version
Distribution	Public	

Table of contents

Table of contents

Project number	
Project acronym	
Project title	CalVal Support System
Annex No.	4.1.3
Title	Enhancement of diffusers BRDF Accuracy for MERIS.
Version	1
Author(s) and affiliation(s)	Bazalgette Courreges-Lacoste NTNO
Modification history	Received 3/9/2006
Distribution	

This short note presents:

1- The synthesis of the calibration work, performed between 1996 and 2002, in four distinct measurements campaigns, on the MERIS on-board diffusers and additional *Spectralon* diffusers dedicated to the calibration of MERIS.

2- The results of the ESA study *Enhancement of diffusers BRDF Accuracy* performed at TNO in 2004-2005.

- **1996 – Characterization of the diffusers in the MERIS calibration grid :**

During the first measurement campaign of 1996, the MERIS qualification model diffusers (i.e. QRR1 and QRR2), the onboard diffusers for MERIS (FRR1 and FRR2), and the ESA diffusers (ESA #21 and ESA #23), were calibrated using the MERIS dedicated setup of TNO allowing out-of-plane measurements for all applicable angles of incidence and observation. After extensive commissioning the accuracy was determined to be < 0.5% (1□) for the absolute BRDF measurements and of the order of 0.3-0.4% for the relative measurements. Parallel to the calibration activity the MERIS test diffuser (#2) was used to quantify the polarization dependence of the BRDF and the specular component both for 65° angle of incidence.

For the used angles of incidence, which lie in the 65° region, and when changing the observation angle within the 68.5° MERIS field-of-view, deviations from ideal Lambertian behaviour were observed to be of the order of 10% (peak-to-peak). However, this non-Lambertian behaviour does not introduce problems as long as the diffusers are carefully calibrated. When varying the wavelength while keeping the geometry fixed, the BRDF was measured to be constant within 1%. Uniformity of the BRDF across the diffuser surface received special attention: for the flight diffusers FRR deviations from perfect surface uniformity were smaller than 0.5% (while the deviation amounts up to 1 % for the qualification model diffusers). An azimuthal dependence of up to 3 % was observed when the azimuth angle was varied from 21.1° to 35.15°.

- **2000 – additional BRDF measurements & characterization of the diffusers out of the MERIS calibration grid :**

In 2000, the MERIS dedicated setup of TNO allowing out-of-plane measurements was updated and used to perform additional BRDF measurements out of the MERIS calibration grid for modelling purpose on the ESA diffuser #23. Also additional BRDF measurements, which were a partial repetition of the previous measurements of 1996, were performed to check the stability of the *Spectralon* diffuser with respect to time. Referring to the error budget as prepared for the MERIS measurements of 1996, the expected error was of 0.5% (1σ) for the absolute BRDF value.

Comparison of BRDF values with the results from 1996 shows that all the values were identical considering a margin +/- 3 σ (1.5 %). From the wavelength scan results, it doesn't appear in the visible and NIR any significant deviation with respect to the measurements of 1996, while a variation of ≈ 1% in the wavelength UV range is present.

- **2000 – Validation of the TNO setup by inter-comparison with NASA GSFC :**

An inter-calibration of the MERIS ESA diffuser #21 was performed between TNO and NASA GSFC in 2000. The comparison of BRDF measurements agreed within 1.5% maximum peak-peak for all angles and wavelength. These measurements are well within the measurement uncertainty (1σ = 0.5 % of the BRDF) of TNO for measurements of 2000 and 2002, within the MERIS spectral range 390-1040 nm.

- **2002 – additional BRDF measurements & space environment degradation of a 2-inch *Spectralon* diffuser :**

In 2002, a new setup (measuring BRDF in the plane of incidence), which was just commissioned and shown compliant with the very strict requirements of OMI, was used to check again the stability of the ESA diffuser (#21 & #23) with respect to time. This measurement setup has the capability of obtaining a BRDF of the MERIS *Spectralon* diffuser with an accuracy of 0.5% (1σ).

The comparison of BRDF values of 2000 measured at TNO for diffuser #23 and #21 with those of 2002 shows that all the values are identical in the range 390-900 nm considering a margin of ± 1 σ. Furthermore, a slight wavelength dependency (≤ 1 %) appears again in the UV range (point at 350 nm) for both diffusers.

The same setup was used to perform some BRDF measurements of the degradation (silicone deposit under UV irradiation) of a 2-inch Spectralon sample propriety of ESA. The most dominant effect of the degradation is a shift of the relative BRDF curve (*i.e.* ratio BRDF after irradiation to the BRDF before irradiation) downwards for wavelength in the UV due to absorption. This is to be expected for a thin strongly absorbing top. An other remarkable effect is the apparent enhanced reflection at large observation angle (observation in the forward scattering direction) that can be due to interplay between absorption and the change of refractive index and/or mean free path.

Finally, in 2002, TNO performed in collaboration with the University of Amsterdam a modelling work of the degradation of the MERIS diffuser in space environment. The effect of the modelled degradation corresponds, in the MERIS geometry, to a shift of the BRDF to the lower values for the UV and visible range. Remarkably, in the NIR spectral range (i.e. 775 nm and 900 nm) the BRDF remains almost constant in the backward scattering direction and even increases in the forward scattering direction.

- **2005 – ESA study *Enhancement of diffusers BRDF Accuracy***

The aim of the study was to improve the BRDF measurement accuracy. For this a set of 5 reflection diffusers and 1 transmission diffuser has been selected on the basis of their space qualification history (aluminium, Spectralon, QVD) or their potential to be on-board of future ESA missions (Fluorion, white tile).

At first the air vacuum effect was measured for the Spectralon diffuser at various angular settings. When comparing the measurement results of the BRDF in air with the BRDF in vacuum no significant difference could be found within the measurement accuracy. When taking the ratio of the two BRDF measurements, differences outside the error margins are observed. A trend can be extracted from the ratio of BRDF measurements recorded in the two environments plotted versus the pressure. From this plot, it can be seen that in the UV region the difference between BRDF measurements recorded in vacuum and in air can go up to a percent for a vacuum of $7x10^{-6}$ mbar. It is thus concluded that the effect of the vacuum on the BRDF of Spectralon diffuser may have an effect on the radiometric calibration of high accurate radiometric instrument (read: instruments with a radiometric budget of 2% or better).

Current state-of-the-art diffuser BRDF measurement accuracy allows to measure absolute BRDF with an accuracy level below 1%. However for some trace gas retrieval techniques, such as DOAS, this accuracy is not sufficient. Since a few years, Scientists are aware that these kinds of retrievals are hampered by an effect known as *Spectral Features*, which is a noise like structure superimposed on the BRDF.

Spectral Features are introduced by the on-board calibration diffuser and are related to the design parameters of the optical system and the scattering properties of the diffuser. To observe this effect, spectral and spatial (partially) coherent light is needed. High-resolution spectrometers provide the spectral coherence and a narrow field of view provides the spatial coherence. Modern space spectrometers have high spectral resolution and a small field of view (high spatial resolution).

In the framework of the ESA study performed at TNO, mechanisms driving the *Spectral Features* effect have been studied and modelled, allowing to provide guidelines and information about the relation of optical instrumentation design and *Spectral Features*. Based on this knowledge the following recommendation to reduce the *Spectral Features* from the point of view of the Instrument optical design can be made:

When a diffuser is used in the instrument *Spectral Features* will occur. Amplitude of the *Spectral Features* is dependent on various parameters, e.g. the instrument design has a prominent role. When *Spectral Features* become too large and endanger the mission measures have to be taken. Although the name *Spectral Features* suggests that they only occur for narrowband spectrometers, also relative broadband detectors (10 nm) can have *Spectral Features* due to the narrow field of view.

There is no simple rule for determining if a mission will suffer from *Spectral Features*. This is depending on the mission radiometric requirements, which drives the instrument design. In general the strategy to reduce *Spectral Features* is to reduce the coherence of the light on the detector. The coherence of the light on the detector is determined by the optical design of the instrument. Parameters such as (instantaneous) field of view and spectral resolution have a strong influence on *Spectral Features*. Unfortunately these parameters are determined by the mission requirements and cannot be changed freely.

The parameters left for the designer to reduce *Spectral Features* are the calibration unit design and the used in-orbit calibration strategy. With respect to calibration unit design the following measures can be taken to reduce the *Spectral Features*:

- Creating a moving source. This can be done by using the movement of the sun position with respect to the diffuser or by moving the diffuser itself. This effect is large in Fourier mode design and fairly small for an imaging mode.
- Using a moving diffuser. If the diffuser is moved during the recording of the spectrum the *Spectral Features* will be averaged out to some extend. In the imaging mode a shift of the diffuser is the best while for Fourier mode a tilt of the diffuser is more efficient.
- Choosing a configuration where a large surface of the diffuser is "seen" by the detector. This leads to small speckles and thereby a large number of speckles per detector pixel.

- Choosing a diffuser with low *Spectral Features*. In this study five diffusers were tested. It shows that a surface diffuser has the worst characteristics, whereas the volume and quasi-volume diffusers show the best characteristics.
- Making a dedicated diffuser design to minimise coherence and therewith *Spectral Features*. The quasi-volume diffuser is an example of this. The design can be optimised for specific wavelength ranges or configurations.

•

Project number	
Project acronym	
Project title	CalVal Support System
Annex No.	4.1.5.
Title	The on-board spectral calibration of MERIS
Version	0.1
Author(s) and affiliation(s)	S. Delwart, ESTEC, ESA
Modification history	17/05/2006
Distribution	Public

The experimental protocol

Calibration of MERIS is performed thanks to the optical concept (see figure 1) at the orbital South Pole (see figure 2) where diffuser plates are deployed by rotating a selection disk into any of the five positions described below:

- Shutter: Will be used for dark calibration as well as for protecting the instrument from contaminants,
- Earth observation**:** A diaphragm is introduced in the field of view.
- Radiometric calibration**:** The sun illuminates a white diffuser plate inserted in the field of view
- Diffuser degradation monitoring**:** A second white diffuser plate will be deployed every 3 months to monitor the degradation of the frequently used plate.

Spectral calibration**:** An Erbium doped "Pink" diffuser will be deployed with MERIS configured to sample its absorption features.

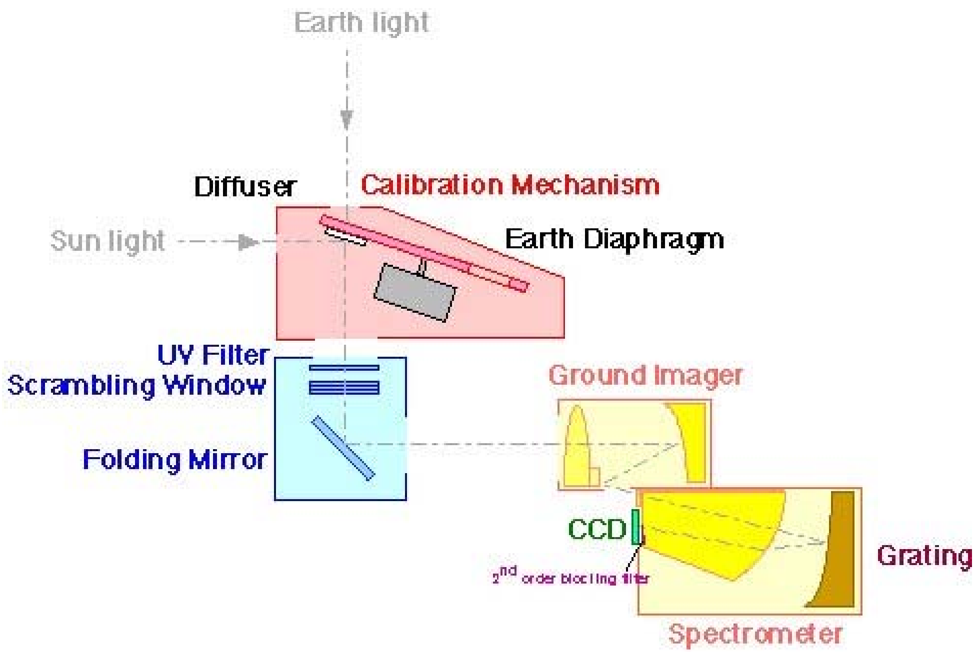

Figure 1: Optical concept

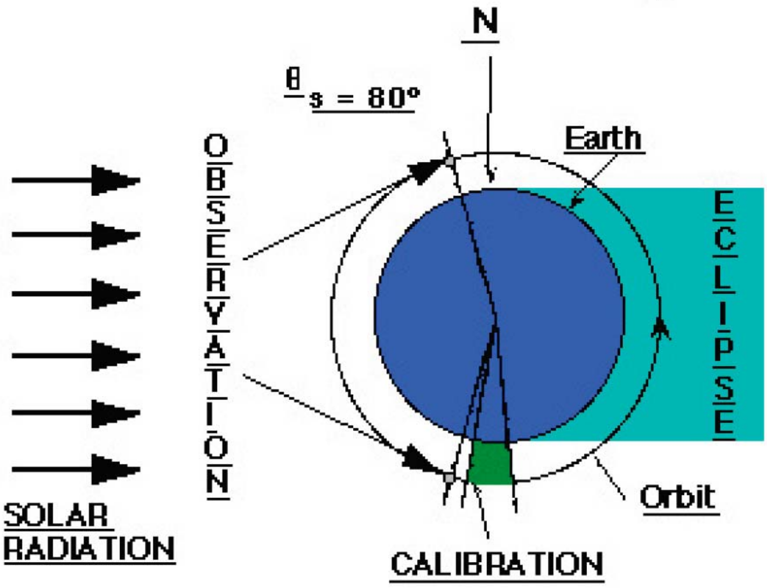

Figure 2: MERIS Operational scenario

The spectral calibration using the on-board Erbium doped diffuser plate is performed in two steps. First, the instrument is configured to have 15 adjacent bands - at the highest spectral resolution - centred on the selected spectral feature (figure 3), and the pixels are calibrated using the radiometric "white" calibration diffuser, the following orbit the “pink” diffuser is deployed and the signal from this spectral feature acquired. Processing on ground determines the position on the detector array of the peak of the Erbium absorption feature.

The absorption peaks (Peak-1 & Peak-3) were selected according to the following criteria: (i) The peak is deep enough, (ii) The peak is narrow enough to be properly covered by 15 adjacent bands spaced at 1.25nm intervals (<18nm) and, (iii) The peaks are separated as much as possible in order to allow for the monitoring of the camera spectral dispersion law.

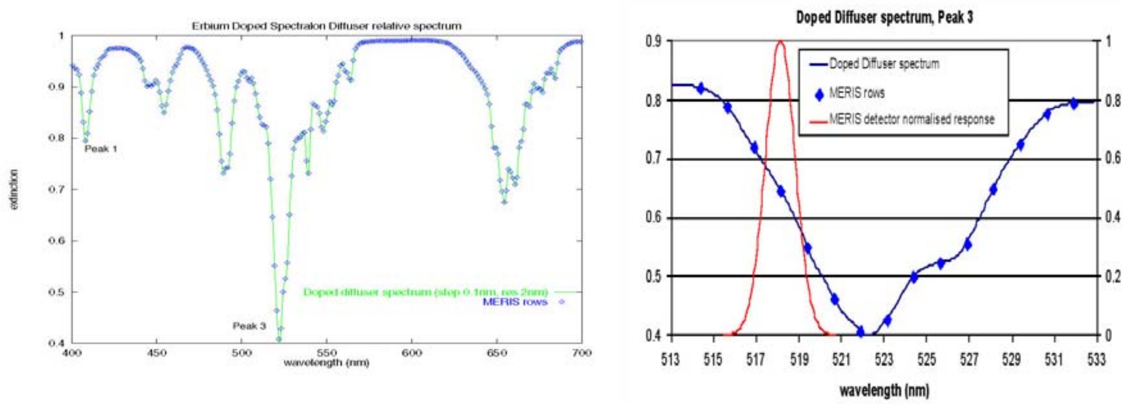

Figure 3: Up: Erbium doped Spectralon^{TM} Diffuser reflection spectrum and instrument spectral band configuration.

References

Delwart S., Preusker R., Bourg L., Santert R., Ramon D., Fischer J., MERIS In-flight Spectral Calibration. Accepted for publication to the International Journal of Remote Sensing.

Project number	
Project acronym	
Project title	CalVal Support System
Annex No.	4.2.1.1.a
Title	The APPEX instrument for calval
Version	0.1
Author(s) and affiliation(s)	Jens Nieke University of Zurich
Modification history	17/05/2006
Distribution	Public

The APEX instrument is an airborne imaging spectrometer to be flown on various aircraft platforms, such as Zeppelin, DO-228, HALO. APEX is an dispersive pushbroom imaging spectrometer operating in the spectral range between 380 - 2500 nm. The spectral resolution will be better than 10 nm in the SWIR and < 5 nm in the VNIR range of the solar reflected range of the spectrum. The total FOV will be ± 14 deg, recording 1000 pixels across track with about 300 spectral bands simultaneously. A large variety of characterization measurements will be performed in the scope of the APEX project, e.g., on-board characterization, frequent laboratory characterization, and vicarious calibration. The retrieved calibration parameters will allow a data calibration in the APEX Processing and Archiving Facility (PAF). The data calibration includes the calculation of the required, time-dependent calibration coefficients from the calibration parameters and, subsequently, the radiometric, spectral and geometric calibration of the raw data.

The APEX instrument has during operations two spectral modes, i.e., a spatial mode (about 300 spectral bands) and a spectral mode (about 500 spectral bands). While for the SWIR channel all 199 can be read-out simultaneously, the APEX VNIR channel has 312 spectral bands, where only 114 bands can be read out in spatial mode, i.e., 312 bands have to be binned in a way that is optimal for various applications, while offering appropriate Signal–to-Noise Ratio (SNR) performance.

For the APEX sensors binning patterns were anaysed recently in order to retrieve best results for the various space sensors simulation (up/down-scaling), such as GLI/SGLI, MODIS or MERIS,

References

Itten, Schaepman, De Vos, Hermans, Schlaepfer, Droz; APEX – Airborne PRISM Experiment: A new concept for an airborne imaging spectrometer, Proc. ERIM, Vol. 1 (1997)

Nieke, Itten, Debruyn, et al., The imaging spectrometer APEX: from concept to realization, eproceedings EARSeL (2005)

Nieke, Honda, Murakami, Takeuchi, Itten, "APEX, a tool for the simulation, calibration and validation of Earth observation sensors", RSSJ Workshop, Naruto, Japan (2005)

Project number	
Project acronym	
Project title	CalVal Support System
Annex No.	4.2.1.1.b
Title	Vicarious calibration in the solar domain using brigth land test sites. Methodology
Version	0.1
Author(s) and affiliation(s)	R. Santer, Université du Littoral, France
Modification history	07/15/2005
Distribution	Public

Characterization of the surface reflectance

It is basically a "reflectance based calibration". There is no need to have a radiometer calibrated in energy. The surface reflectance, in a given spectral band j, is derived from a cross comparison between measurements over the test site and over a reference panel. Ideally, the radiometer is equipped with the same spectral bands than the satellite sensor to calibrate. For a given spot on the surface, i,, the surface reflectance $\rho_{i,j}^{g}$ is given by:

$$\rho_{i,j}^{g}(\theta_v^g, \theta_s, \varphi^g) = \rho_j^p(0, \theta_s).DC_{i,j}^g / DC_j^p \quad (1)$$

The reflectance of the panel $\rho_j^p(0, \theta_s)$ is generally known for a nadir view versus the incident angle. Implicitly, it is also assumed than the solar angle θ_s represents the mean incident direction for the total irradiance. It is strictly true for the direct irradiance; and the diffuse light is assumed to be in mean distributed around the incident solar direction. Surface and panel measurements are not simultaneous. Therefore the incident downward fluxes differ. Two panel measurements bound a series of surface measurements and a relevant interpolations in θ_s (or cosine (θ_s)) is done on DC_j^p to have a correct estimation of the incident downward flux at the time of the surface measurement.

The geometry $(\theta_v^g, \theta_s, \varphi^g)$ of the surface reflectance measurement ideally corresponds to the geometry of the satellite measurement. On a practical point of view, surface reflectance measurements are done as well at nadir. A standard bidirectional model of the surface is assumed for this correction.
To account for the spatial heterogeneity of the test site, the surface reflectances are measured, around the time of overpass, over the test site with a sampling protocol adapted to the site heterogeneity. The less homogeneous the site is, the more measurements you need to collect. These reflectances are then spatially averaged.

Characterization of the aerosols

The main parameter is the aerosol optical thickness τ_a measured at the satellite time of overpass. Most of the time, there is a need to spectrally interpolate the ground based measurements to the satellite spectral bands. The Junge size distribution is generally used:

$$n(r) = \frac{dN}{dr} = Cr^{\nu}, \qquad (2)$$

with ν the Junge parameter, directly related to the Angström coefficient by:

$$\upsilon = \alpha - 3. \qquad (3)$$

The refractive index of the particles is taken from the local climatology and the particle shape is assumed to be spherical in order to apply the MIE theory.

Auxiliary atmospheric parameters

The Rayleigh scattering depends upon the Rayleigh optical thickness τ_R , proportional to the barometric pressure
Ozone amount is provided by different sources, default is the climatology. Water vapour content is generally measured at the surface level. Radiosondes may also be available to give the vertical profile.

Simulation of the satellite signal

A radiative transfer code (RTC) is used with the surface reflectance as boundary condition. The atmospheric inputs are the barometric pressure (to compute the Rayleigh scattering) and the aerosol model. Generally, a first run with a RTC is done to compute the radiance ignoring the gaseous absorption. Then only the gaseous transmittance is computed. Scattering and gaseous absorption are then decoupled. Outputs are combined to predict the incoming reflectance (normalized radiance, Es=π) for each sensor band. Digital counts are extracted for the test site. The calibration equation is applied. The general flow chart is given in figure 2.

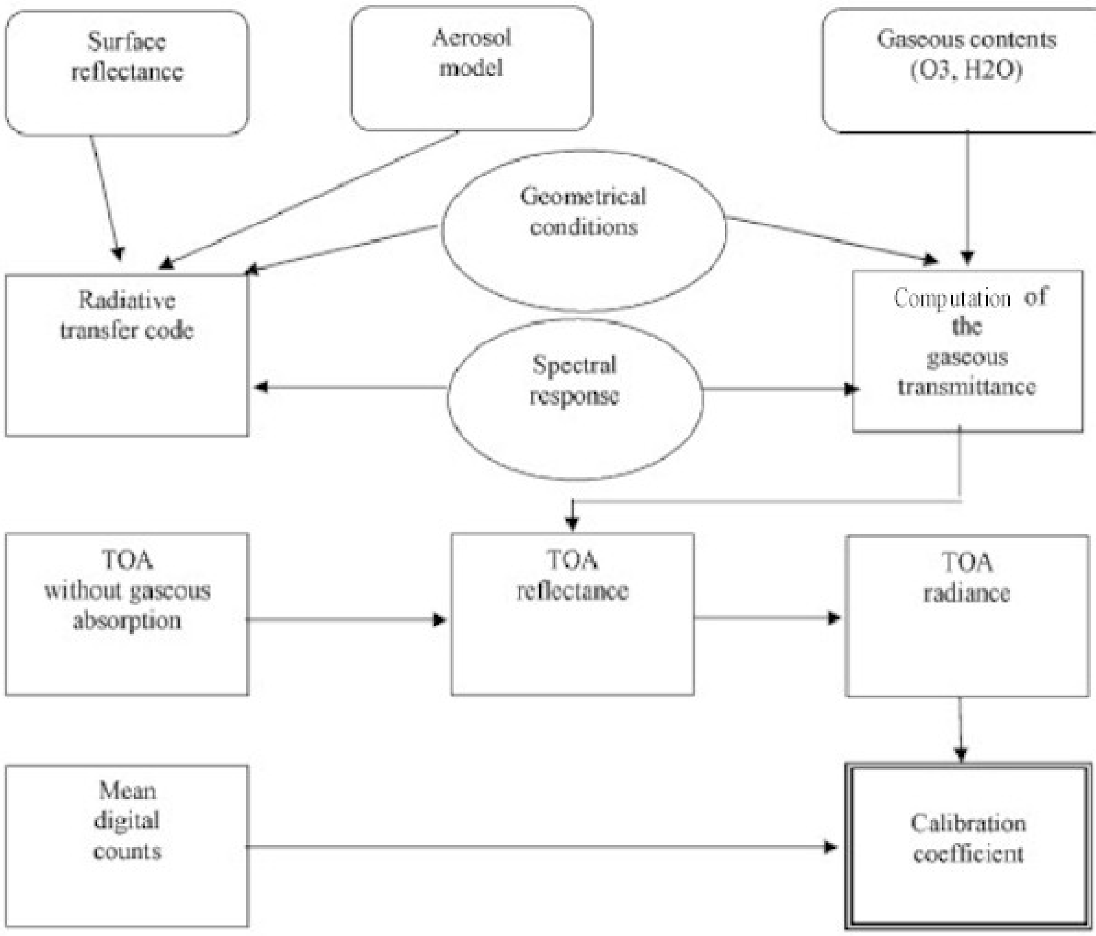

Fig. 2 : Flow chart for the vicarious calibration

References

1. P.N. Slater, G. Begni, M.C. Dinguirard, and R.D. Jackson, « Absolute calibration of the SPOT-1 HRV cameras », vol. 660 *Earth Remote Sensing Using the Landsat Thematic Mapper and SPOT-sensor Systems*, 1986.

2. R. Santer, X. Gu, J.L. Deuzé, C. Devaux, E. Vermote, et al., « SPOT calibration at the La Crau test site (FRANCE) », *Remote Sensing of Environment* 41:227-237, 1992.

Project number	
Project acronym	
Project title	CalVal Support System
Annex No.	4.2.1.2
Title	Vicarious calibration in the solar domain using brigth land test sites: The La Crau site
Version	1.0
Author(s) and affiliation(s)	R. Santer Université du Littoral
Modification history	First draft,
Distribution	

La Crau is a flat plain of 20 kilometre diameter, cover by white pebbles, and located in the south east of France. It is a public domain accessible all over the year. This homogeneous bright site is used by CNES since 1987 as a test site for vicarious calibration of the SPOT-HRV cameras. Pictures from the sites are reported in figure 1. A 300 mx 300 m was selected (see figure 1 (b)) for the SPOT calibration. Indications on the spatial homogeneity are reported in table 1.

The typical reflectances reported in figure 2 indicate a medium bright site. Figure 3 is a statistical view of the surface reflectances in the three SPOT_HRV bands. The dispersion of the surface reflectance is quite high which implies to measure these reflectances for vicarious calibration. The bidirectional reflectances were measured. Figure 4 illustrate the bidirectionality of the reflectance. Such information is used to convert surface reflectance measurements at nadir into surface reflectance in the satellite sensor view geometry.

La Crau is free of clouds more than 200 days a year. Under clear conditions, Figure 6 reports the aerosol optical depth at 550 nm and the Angstroem coefficient. Typical horizontal visibility is 23 km with very clear days when a strong local wind (Mistral) blows.

References

Gu X.F. Étalonnage et intercomparaison des données satellitaires en utilisant le site test de La Crau. *Thèse de doctorat de l'université Paris VII.*

Gu X.F., Guyot G., Verbrugghe M., 1992 ; Evaluation of measurements errors in ground surface for satellite calibration. *International Journal of Remote Sensing*, ***13****(14):2531-2546*

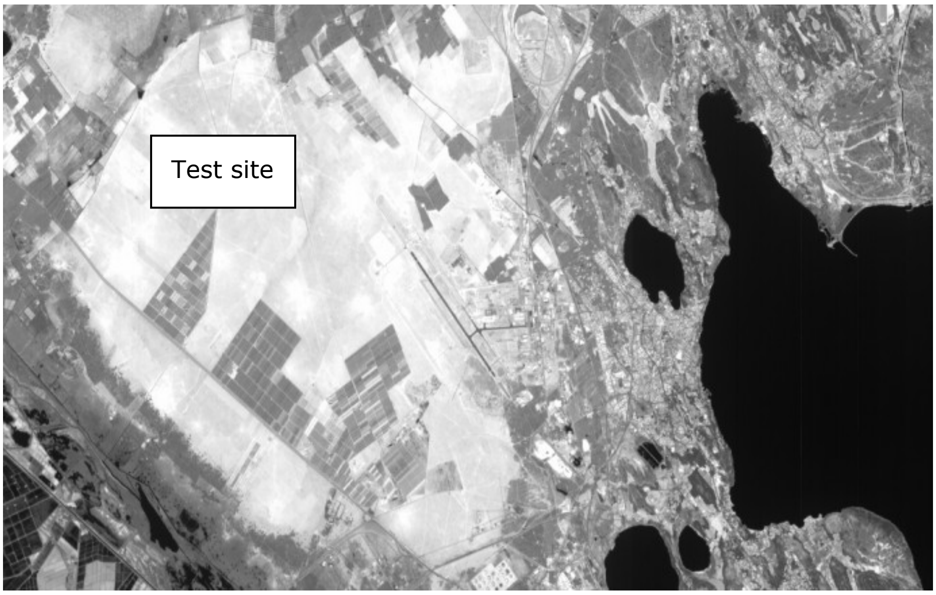

(a)

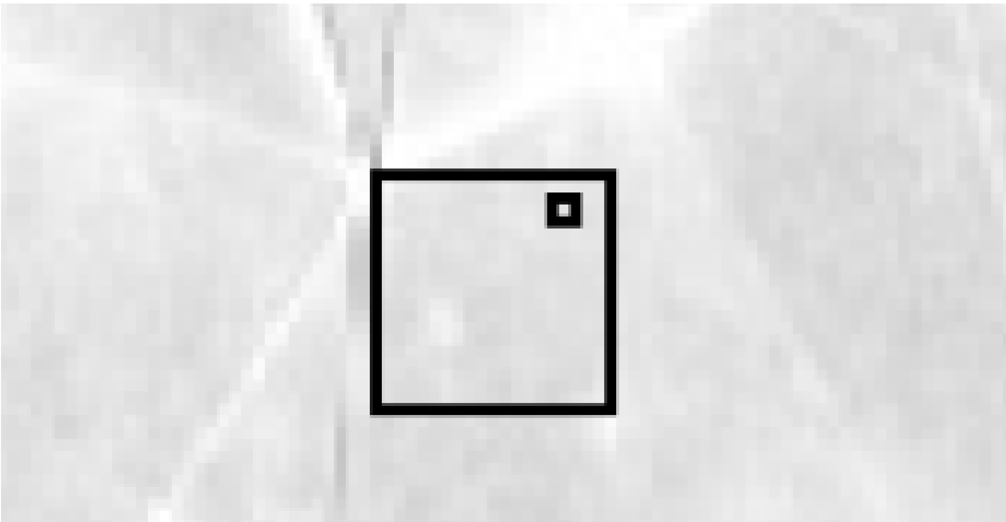

(b)

©

(d)

Figure 1: La Crau from (a) SPOT-HRV, (b) a zoom in HRV-B3, (c) from the surface, (d) a zoom at nadir.

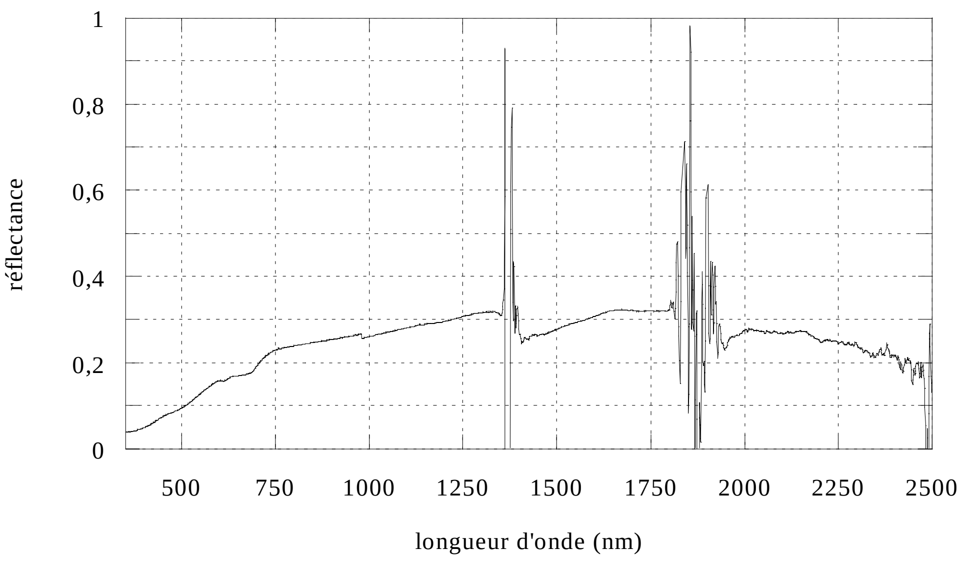

Figure 2: Typical spectral signature of the La Crau surface reflectance.

λ (nm)	380	440	550	870
ρ	0.03	0.05	0.12	0.24

Table 1: Typical values of the La Crau surface reflectance

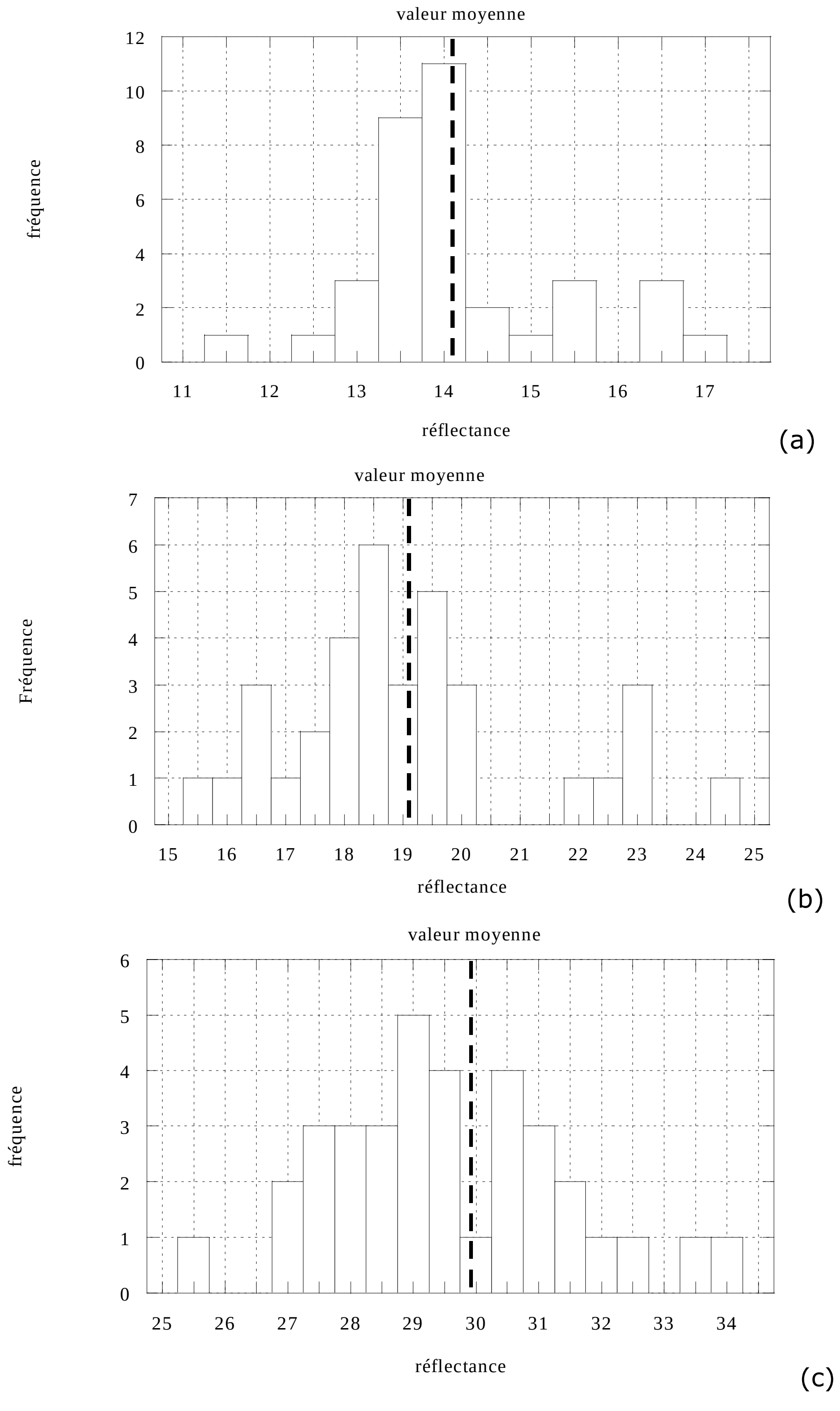

Figure 3: Histogram of the La Crau reflectance in the SPOT-HRV bands: (a) B1 at 550 nm, (b) B2 at 650 nm, (c) B3 at 865 nm. Data were collected during fiel campaigns between 1989 and 1997.

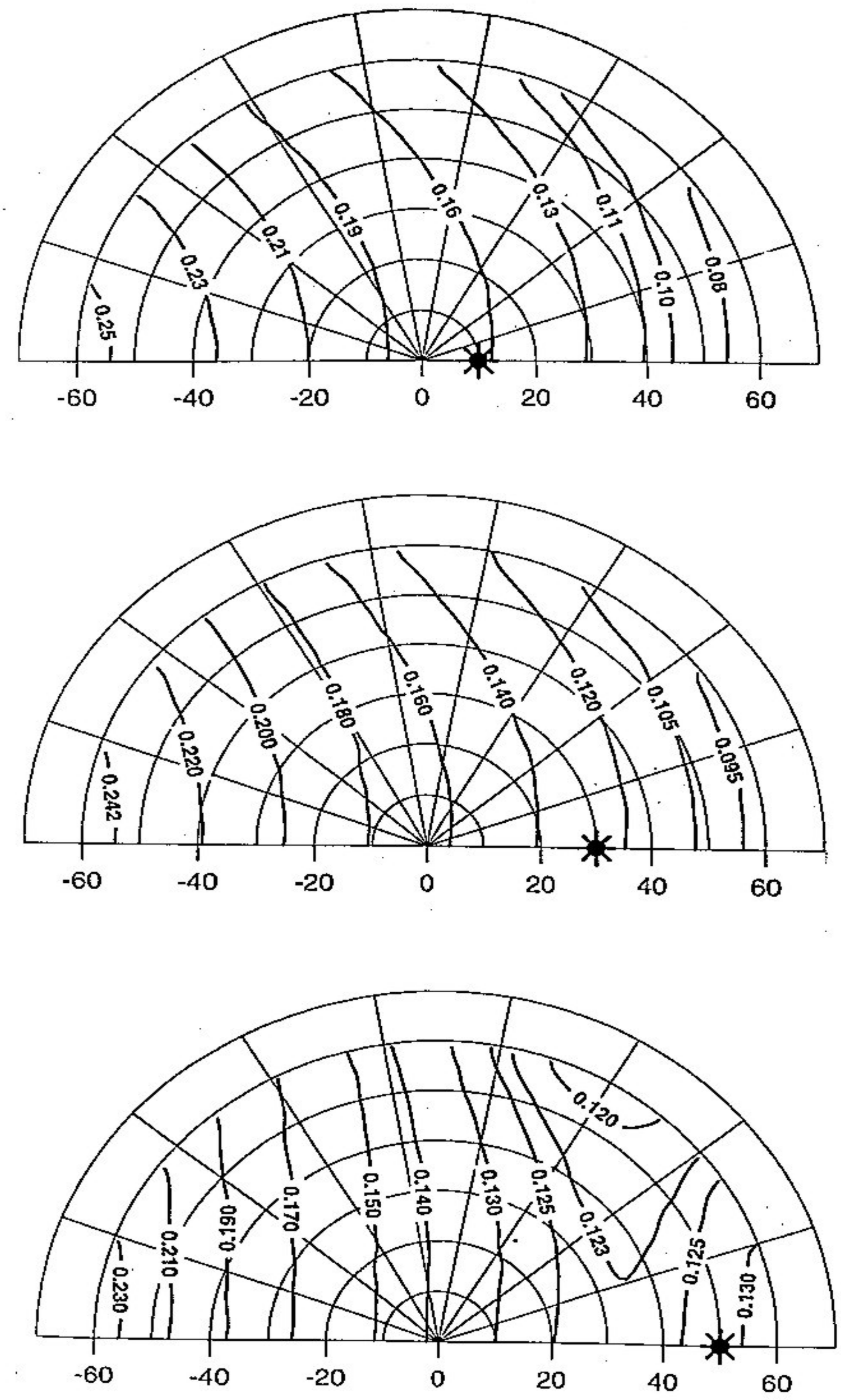

Figure 4: Polar diagram of the La Crau reflectance at 650 nm at three solar angles. Solar position is reported on the x-axis.

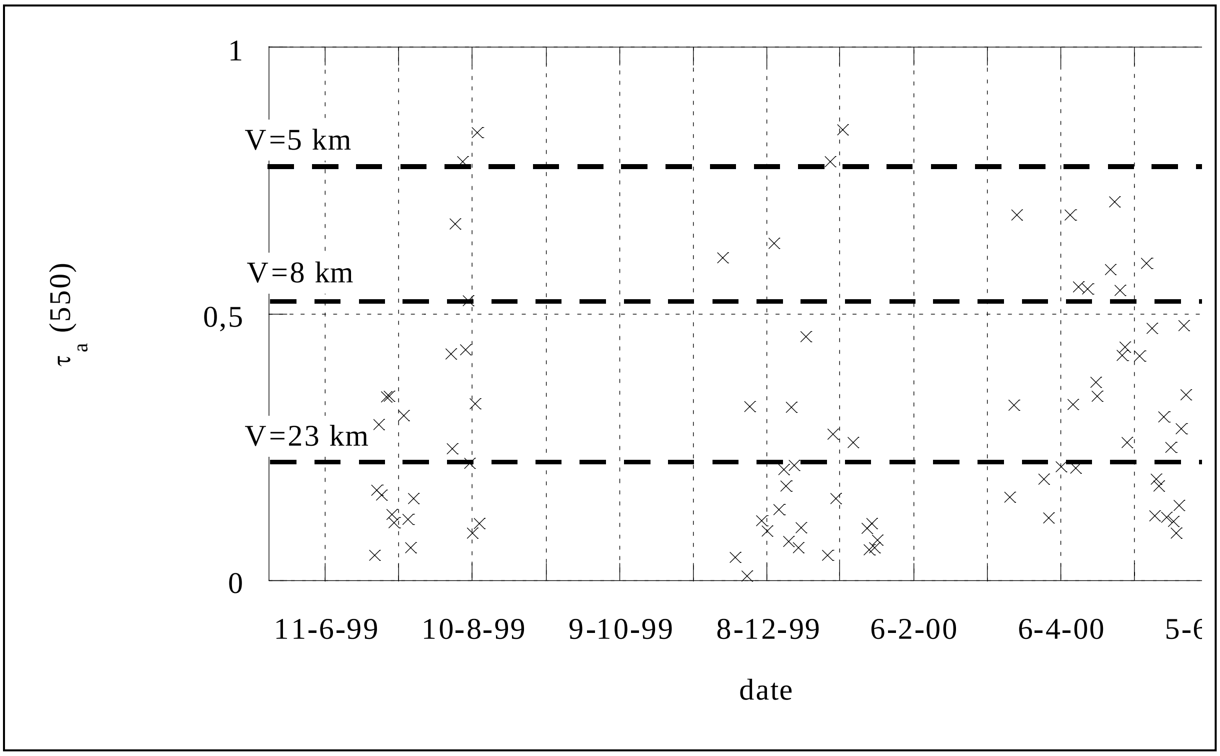

(a)

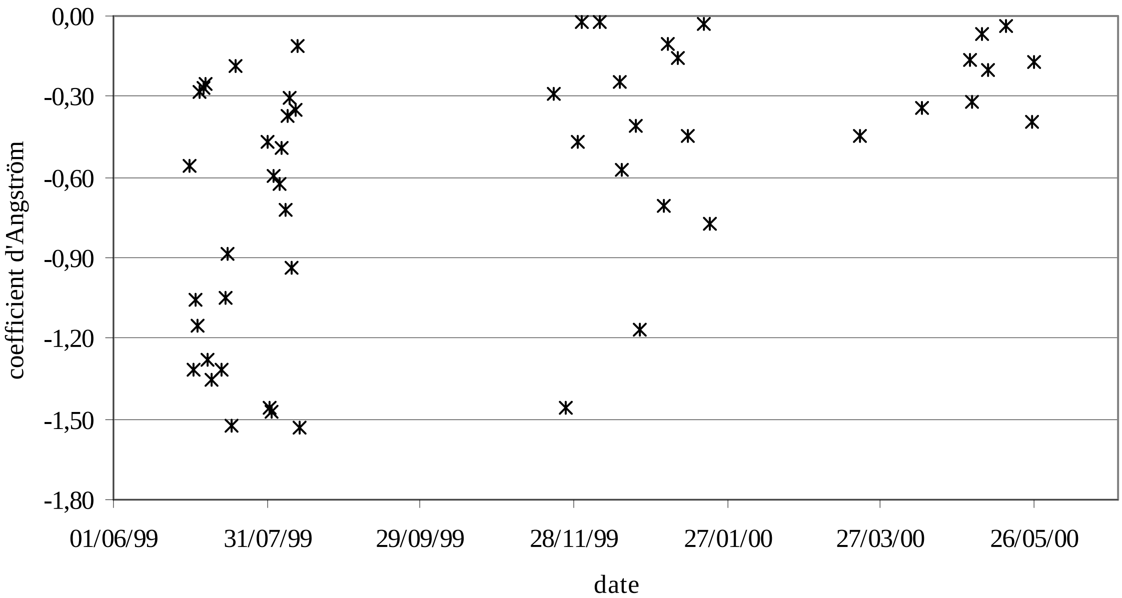

(b)

Figure 5: Histogram of the La Crau reflectance in the SPOT-HRV bands: (a) B1 at 550 nm, (b) B2 at 650 nm, (c) B3 at 865 nm. Data were collected during field campaigns between 1989 and 1997.

Project number	
Project acronym	
Project title	CalVal Support System
Annex No.	4.2.2.1 a
Title	Radiometric Calibration in the Red and Near Infrared
Version	
Author(s) and affiliation(s)	R. Frouin, Scripps Institution of Oceanography R. Santer, Université du Littoral
Modification history	3/1/2006
Distribution	Public

Principle

Outside of the sunglint, the open ocean is dark in the near infra red if the wind speed is low enough to neglect the contribution of the foam reflectance. The only contributor to the satellite signal is the atmospheric scattering. Molecular scattering is known from the surface pressure. The aerosol characterization is the key issue. An accurate radiative transfer code may be used to solve the radiation-transfer equation and predict the TOA radiance, L_{TOA}. The input variables of the radiation-transfer code to compute L_{TOA} are the aerosol optical thickness, the "pseudo" aerosol phase function, and the surface wind speed.

The scattering properties of the aerosols may be obtained using data from CIMEL radiometers of the Aerosol Robotic Network (AERONET) (Holben et al., 1998). The arerosol phase function is computed knowing the aerosol model (size distribution and refractive index). Alternatively, it is possible to determine directly the aerosol optical properties. Using the algorithm developed by Wang and Gordon (1993) to estimate aerosol phase function and single scattering albedo, Gordon and Zhang (1996) showed that the top-of-atmosphere radiance can be predicted with an accuracy of 1-2% in the near infrared (if the surface radiometer is perfectly calibrated). A variant of this method was proposed recently in Santer and Martiny (2003). Instead of iterating directly over phase function and single scattering albedo, the measured sky radiance is first corrected for multiple scattering effects. The "pseudo" phase function, i.e., the product of phase function and single scattering albedo, is then obtained immediately using the primary scattering formulation. The process is repeated once to improve the correction of multiple scattering and, therefore, the determination of the "pseudo" phase function. Both studies concluded that the most important source of error in the prediction of the top-of-atmosphere radiance is the accuracy of the sky radiance.

Application to SeaWiFS calibration in the near infrared

The calibration method has been applied to the calibration of SeaWiFS in the near infrared (band 8, centered at 865 nm) (Martiny et al., 2005). CIMEL data acquired at two locations were used, from a platform off Venice, Italy, and from a site on the west coast of Lanai, one of the Hawaiian Islands, near the MOBY buoy site. 26 days have been selected for the calibration study: 19 for the Venice site and 7 for the Lanai site.

Using for the analysis the days with at least two phase-function retrievals, i.e. 20 days out of 26 days, the TOA L computations have indicated that the SeaWiFS radiance in band 8, as provided by the SeaWiFS Project Office, is biased low by 7.0% ± 2.8% (Figure 1). No significant dependence on aerosol optical thickness and scattering angle is detected.

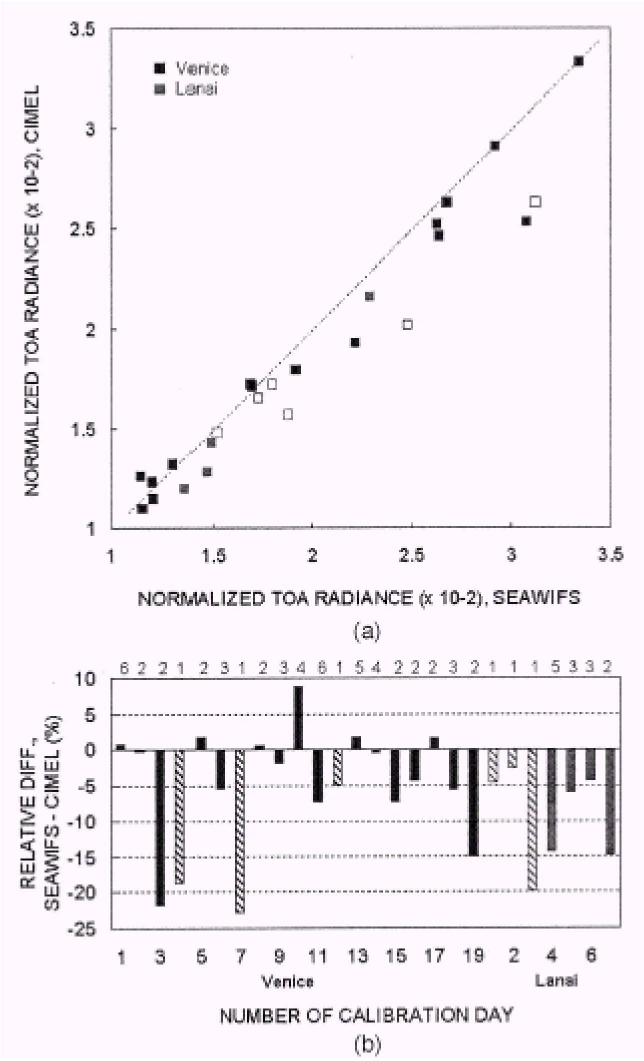

Figure1. SeaWiFS radiometric calibration in the near infrared (band 8), for the 19 days selected for the Venice site and the 7 days selected for the Lanai site. (a) CIMEL-retrieved TOA radiance versus SeaWiFS TOA measurements. (b) Relative difference between SeaWiFS measurements and CIMEL retrievals. Labels on the top represent the number of principal plane sets used for the computation of the TOA radiance. (After Martiny et al., 2005.)

We can provide an alternative, purely radiometric "vicarious" calibration to the "entire system" calibration routinely performed by the SeaWiFS Project Office, which does not separate sensor from algorithms. A fairly automated radiometric calibration system based on the proposed methodology and exploiting the remote acquisition of CIMEL data from island and coastal sites around the globe, might be envisioned. It would allow one to check and monitor operationally, at relatively low cost, the absolute calibration of current and future satellite ocean-color sensors in the red and near infrared, where the ocean can be considered black, while they operate in orbit.

Project number	
Project acronym	
Project title	CalVal Support System
Annex No.	4.2.2.1 b
Title	The Acqua Alta Oceanographic Platform (AAOT) Site
Version	
Author(s) and affiliation(s)	Giuseppe Zibordi and Jean-François Berthon Joint Research Centre, Ispra
Modification history	
Distribution	

The Acqua Alta Oceanographic Tower (AAOT) is located the northern Adriatic Sea, 8 nautical miles offshore the Venice lagoon (45.314°N, 12.508°E). At this site the average water depth is approximately 17 m and the sea bottom is mostly composed of sand and mud. The AAOT is owned and managed by the Italian National Research Council and its is used to support ocean color calibration and validation activities within the framework of the Coastal Atmosphere and Sea Time-Series (CoASTS) program (Zibordi et al. 2002). Peculiarity of the AAOT is its position in a frontal region characterized by succession of Case-1 and Case-2 waters making the site well representative of coastal zones (here defined as regions permanently or occasionally affected by bottom resuspension, coastal erosion, river inputs, or by relevant anthropogenic impact). The site exhibits an occurrence of roughly 60% Case-1 waters (Berthon et al. 2002) identified according to Loisel and Morel (1998).

Figure 1. Picture of the AAOT.

References

J.-F. Berthon, G. Zibordi, J. P. Doyle, S. Grossi, D. van der Linde, C. Targa, "Coastal Atmosphere and Sea Time Series (CoASTS), Part 2: Data analysis". NASA Tech. Memo. TM-2002-206892, S.B.Hooker and E.R.Firestone, Eds., NASA Goddard Space Flight Center, Greenbelt, Maryland, vol. 20, pp. 1-25, 2002.

H. Loisel and A. Morel, "Light scattering and chlorophyll concentration in case 1 waters: A reexamination," *Limnol. Oceanogr.*, vol. 43, pp. 847–858, 1998.

G. Zibordi J.-F. Berthon, J. P. Doyle, S. Grossi, D. van der Linde, C. Targa, L. Alberotanza, "Coastal Atmosphere and Sea Time Series (CoASTS), Part 1: A long-term measurement program," NASA Tech. Memo. 2002-206892, S.B.Hooker and E.R.Firestone, Eds., NASA Goddard Space Flight Center, Greenbelt, Maryland, vol. 19, pp. 1-29, 2002.

Project number	
Project acronym	
Project title	CalVal Support System
Annex No.	4.2.4.2
Titl	Intercomparison of imaging spectrometers over the Salar De Uyuni (Bolivia)
Version	1
Author(s) and affiliation(s)	M. Bouvet
Modification history	Received 19/05/2006
Distribution	Public

1. INTRODUCTION

The lack of in-situ measurements describing the atmosphere/surface physical state is a strong limitation when trying to achieve *absolute calibration* over natural targets. Workarounds exists to cope with the lack of in-situ data availability and still be able to retrieve pertinent information. There are, in fact, vicarious calibration methodologies that can be referred to as *intercalibration* methodologies for which several sensors data are intercompared over a bright natural target and one of the sensors is arbitrarily chosen as a reference (R 2, R 1*).* This type of methodology, if operationally implemented, can provide long time series of relative differences in instrument calibration that can be nailed down to an absolute reflectance scale by episodic absolute calibration experiments. Hereafter is presented an attempt to identify trends over nearly 4 years of operations in the relative differences of radiometric calibration between A-MODIS, AATSR MERIS, POLDER-3 and SeaWiFS. The natural target chosen for this intercomparison is the *Salar de Uyuni* (Bolivia). It was selected for its spectrally white high reflectance, its flatness, its high altitude location and its dry climate. In the next section, the details of the methodology are described. Then, the results are presented and discussed.

2. METHODOLOGY

2.1. The methodology

The goal of the methodology could be simplistically summarized as follow: *to identify radiometric calibration differences between two different sensors by looking at the same terrestrial target from the top of the atmosphere, at the same time and in the same geometrical configuration*. L1B radiance/reflectance data in all available bands spanning from the 400 nm to 1020 nm are systematically extracted from A-MODIS, AATSR, MERIS, POLDER-3 and SeaWiFS data over a region of interest of dimensions 20 km by 60 km centered on the *Salar de Uyuni*, in Bolivia. The data are then visually cloud screened and converted to a common radiometric scale (when needed): the remote sensing reflectance. This conversion is carried with the help of the extraterrestrial spectral irradiance spectrum specific to each mission and the Relative Spectral Responses (RSR) of each band from each instrument. For each acquisition from each sensor, the reflectances in all spectral bands, the sun zenith angle (SZA), the viewing zenith angle (VZA) and the viewing azimuth angle relative to the principal plane (RAA) are average over all pixels included in the region of interest and systematically stored.

Then, doublets between two sensor acquisitions *i* and *j* are searched which have comparable geometries of observation and illumination. To look for such doublets, it is assumed that the TOA reflectance angular distribution obeys a) the principle of reciprocity and b) is symmetrical with respect to the principal plane. The principal of reciprocity states that the following relationship is true:

$$\rho_i^{TOA}(SZA_i, VZA_i, RAA_i) = \rho_j^{TOA}(VZA_j, SZA_j, RAA_j) \quad (1)$$

while the symmetrical assumption with respect to the principal plane can be formulated as:

$$\rho_i^{TOA}(SZA_i, VZA_i, RAA_i) = \rho_j^{TOA}(SZA_j, SZA_j, -RAA_j) \quad (2)$$

Because an exact geometrical match is often not possible, the search for such geometrical configuration is actually carried out by looking for acquisitions between the sensor *i* and the sensors *j* satisfying the condition $\chi_{ij}<10$ where χ is defined as:

$$\chi_{ij} = \sqrt{\left([SZA_i - SZA_j]^2 + [VZA_i - VZA_j]^2 + \frac{1}{4}[|RAA_i| - |RAA_j|]^2\right)} \quad (3)$$

$\chi_{ij}<10$ roughly corresponds to configurations for which the SZA's, the VZA's do not differ by more than 5° and the RAA's by more than 10°.

Moreover, only doublets of two sensors that satisfy the geometrical criteria of equation (3) and for which the acquisition were performed on the same day or one day apart are kept in the final dataset. This implicitly equivalent to assuming that the TOA reflectance Bidirectional Reflectance Distribution Function (BRDF) does not vary significantly over 24 hours.

Finally, if for a given acquisitions of sensor *i*, there exists several acquisitions from sensor *j* satisfying the previous geometrical and temporal criteria, then only the matching acquisition from sensor *j* for which the χ_{ij} is the smallest is kept to form a doublet with the acquisition of sensor *i*.

2.2. Site characteristics and climatology

The Salar de Uyuni (Bolivia) is a salt lake located at approximately 20 degree South latitude and 68 degree West longitude (*Figure 1*). Only a marginal part of its surface remains wet during the dry season (March to November) thus leaving large areas of dry and highly reflective salt. In its largest dimension, it extends by approximately 200 km. It is a plateau lying at an altitude of 3600 m.

The rain season starts in December and ends up in March. The lake surface is then flooded for few months. From data obtained at a meteorological station located East of the dry lake, operated during over 13 years between 1987 and 1999 (R 3), the average precipitation is nearly null from May to October. For the same period of the year (dry season), the averaged number of rain days per month over 13 years is between 0 and 2. Mean temperatures oscillate between 14 degrees in December and 2 degrees in June.

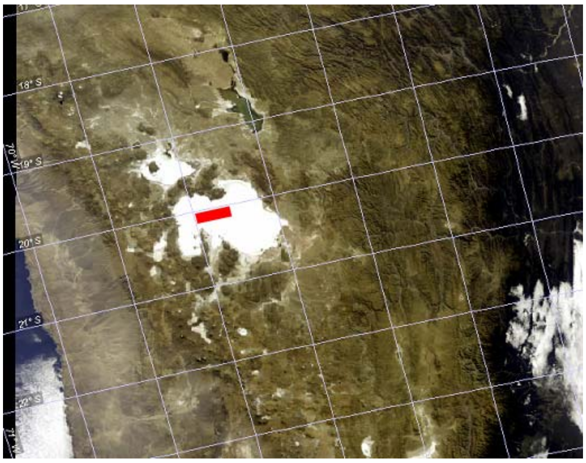

Figure 1: The Salar de Uyuni (Bolivia) as observed by MERIS on the 10th of June 2005. The region of interest chosen for intercomparison of TOA reflectances lies between latitudes -20.16 and -20.00 degree latitude and -68.05 degree and -67.45 degree longitude.

Salar de Uyuni is a large, flat and radiometrically homogenous area.

Authors of R 3 carried out ground reflectance measurements with a LICOR LI-1800 spectrometer and obtained average reflectance spectrum smoothly increasing from 70 % to 80 % between 400 nm and 900 nm. This spectrum was extracted in the area considered in the present intercomparison study. If looking at the surface at different wavelength can expect spectral reflectance gradients of about 0.025 % / nm.

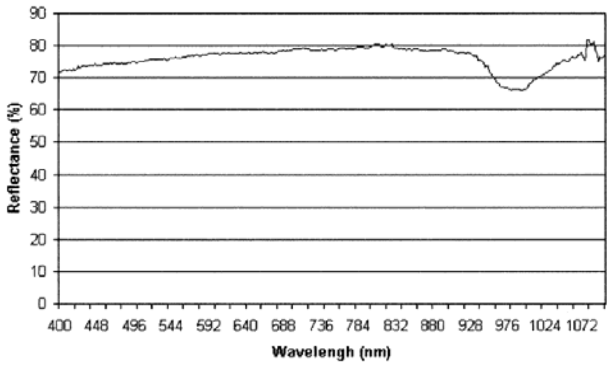

*Figure 2: Mean ground reflectance spectrum measured with the spectroradiometer LICOR LI-1800 on June 8 and June 9, 1999 (*R 3*)*

This spectral flatness minimizes differences when comparing reflectances from sensors having relative spectral responses (RSR) differing in their width or wavelength center.

The high altitude of the *salar* implies a rarefied molecular atmosphere. Pressure is approximately reduced to two thirds of the mean sea level pressure, consequently reducing the Rayleigh scattering optical thickness and thus the atmospheric influence on the downwelling and upwelling radiation field.

An interesting characteristic of a salt lake such as the *Salar de Uyuni* is that it should have a smooth BRDF and as a consequence, the differences in measured TOA reflectances when observing its surface under closely related geometries should be minimized.

2.3. The satellite data

The satellite data consist of L1B data, i.e., radiometric and geolocation/navigation data. The TOA reflectances are extracted systematically from overpasses and are further visually cloud screened. All data starting from 2002 and finishing in 2005 are included when available thus resulting in maximum 4-year time series.

For each sensor, the final radiometric quantities extracted are TOA reflectances in all spectral bands spanning from 400 nm to 1000 nm. When not available directly as reflectances, the TOA radiometric quantities (radiances or normalized reflectances) are converted into reflectance via the appropriate extraterrestrial solar irradiance E_0 and knowledge of the sun zenith angle. The final radiometric quantity thus compared is the remote sensing reflectance:

$$\rho^{TOA} = \frac{\pi L^{TOA}}{E_0 \cos(SZA)} \quad (4)$$

The Sun Zenith Angle (SZA), Sun Azimuth Angle (SAA), Viewing Zenith Angle (VZA), Viewing Azimuth Angle (VAA) were also extracted from the auxiliary navigation data in the L1B files and similarly to the TOA reflectances, they were averaged over the region of interest (*Figure 1*).

The results given by such methodology together with a discussion on its applicability can be found in **Bouvet M.** (2006), Intercomparison of imaging spectrometers over the Salar De Uyuni (Bolivia), *Proceedings of the 2006 MERIS AATSR Validation Team workshop*

3. REFERENCES

R 1 Bouvet M., S. Delwart, Imaging spectrometers comparison over snow – A case study over Longyearbyen on the 3rd of May 2003, *Envisat MAVT 2003 proceedings*

R 2 Cosnefroy, H, Soule, P., Briottet, X., Hagolle, O., Cabot, F. POLDER multiangular calibration using desert sites: method and performances, Proceedings of SPIE Volume: 3221, 1997

R 3 Lamparelli Rubens Augusto Camargo, Flávio Jorge Ponzoni, Jurandir Zullo, Jr., Giampaolo Queiroz Pellegrino, and Yves Arnaud, Characterization of the Salar de Uyuni for In-Orbit Satellite Calibration, *IEEE TRANSACTIONS ON GEOSCIENCE AND REMOTE SENSING*, VOL. 41, NO. 6, June 2003

Project number	
Project acronym	
Project title	CalVal Support System
Annex No.	4.2.6.1
Title	Fraunhoffer spectral calibration
Version	0.1
Author(s) and affiliation(s)	R. Preusker and J. Fischer Freie Universität Berlin
Modification history	07/03/2006
Distribution	Public

Principle and algorithm

The **Fraunhofer lines** are a set of spectral lines named for the German physicist Joseph von Fraunhofer (1787-1826). The lines were originally observed as dark features in the optical spectrum of the Sun. The English chemist William Hyde Wollaston was in 1802 the first person to note the appearance of a number of dark features in the solar spectrum. In 1814, Fraunhofer independently rediscovered the lines and began a systematic study and careful measurement of the wavelength of these features. In all, he mapped over 570 lines, and designated the principal features with the letters A through K, and weaker lines with other letters. It was later discovered by Kirchoff and Bunsen that each spectral line was associated with a chemical element, and deduced that the dark lines in the solar spectrum were caused by absorption by those elements in the upper layers of the sun. Some of the observed features are also caused by absorption in oxygen molecules in the Earth's atmosphere.

Wavelength (nm)	Bandwidth (nm)	**Element**
393.3682	2.0253	Ca II[2]
396.8492	1.5467	Ca II
410.1748	0.3133	H
434.0475	0.2855	H
486.1342	0.3680	H
518.3619	0.1584	Mg I
656.2808	0.4020	H
849.8062	0.1470	Ca II
854.2144	0.3670	Ca II
866.2170	0.2600	Ca II

Table 1: Major Fraunhofer lines and associated elements.

The Fraunhofer C-, F-, G'-, and h- lines correspond to the alpha, beta, gamma and delta lines of the Balmer series of emission lines of the hydrogen atom (see table 1). The D_1 and D_2 lines form the well-known "sodium doublet", the centre wavelength of which (589.29 nm) is given the designation letter "D".

Because of their well defined wavelengths, Fraunhofer lines are predestined to characterize the wavelengths of measured spectra in the visible and near infrared. We selected a number of strong Fraunhofer lines which can be detected with the MERIS instrument.

For the MERIS spectral calibration we choose the Fraunhofer lines at 395nm, 486nm, 595nm, 656nm, 854nm and 866nm (see Table 2 and Figure 1). The algorithm is divided into identical parts for each used Fraunhofer line. It is based on a look up table (LUT), which contains normalized radiance L_{norm} :

$$L_{norm} = \frac{L}{\max(L_{meas})}$$

These normalized radiances are computed as a function of the centre wavelength of the MERIS micro channels. The distance between the channels and the bandwidth of the micro channels are assumed to be known.

The matching entry in the LUT is found by minimizing *d*

$$d = \sqrt{\frac{\sum_i^n (L_{norm} - L_{LUT})^2}{n}}$$

which is the distance between the LUT entries and the normalized measurements; *n* is the number of used micro-channels around the Fraunhofer line. The reflected radiation at the white diffuser plate is used for the calibration.

During the calibration campaigns, the 15 MERIS channels has been changed by programming the satellite instrument, that the 15 channels covers selected Fraunhofer lines with the highest possible spectral resolution of nominal 1.25 nm.

Data and Results

Table 3 describes three different spectral calibration campaigns. Since the maximal number of transmitted micro-channels is 15 and the spectral range of each set of micro-channels has to cover the Fraunhofer lines with all cameras, we have defined campaigns with different sets of micro-channels to check the spectral accuracy of the entire spectral range of MERIS. To cover the near infra red, the two Fraunhofer lines at 866 nm and 854 nm have been used. The strong line at 396 nm has been used, but due to the sensitivity of the sensor only a limited accuracy can be achieved with respect to spectral accuracy. However, at 396 nm the spectral calibration appears well defined because the absorption line is quite strong. Conversely at 866 nm, the spectral calibration is less precise. In order to give some estimate of the method accuracy, we computed the standard deviation for camera 3 after a linear regression on the spectral shift. Results are reported in table 3.

Campaign	Orbits	Dates	Fraunhofer lines (number of micro-channels)
Fall 2002 I	3598,3602,3603,3696	07, 14. Nov. 2002	585(5),656(5),866(5)
Fall 2002 II	3611,3609	08 Nov. 2002	396(7),486(4),854(4)
Spring 2002	0713,0718,0719	09, 20 Nov. 2002	396(5),486(3),656(3),854(4)

Table 2: The Fraunhofer lines calibration campaigns; the wavelengths are in nm and the number of MERIS micro-channels are in brackets.

λ (nm)	396	486	585	656	854	866
Δλ (nm)	0.022	0.026	0.078	0.027	0.079	0.105

Table 3: The accuracy of the Fraunhofer calibration in different absorption band as the standard deviation of a linear regression for camera 3

Summary

The spectral calibration of the MERIS instrument using the well defined Fraunhofer lines is accurate by 0.025 nm for the stronger lines and around 0.1 nm for the weaker lines. The is sufficient to characterise the instrument and to account for the smile effect the MERIS instrument. The spectral calibration by means of measuring selected Fraunhofer lines is accomplished twice a year.

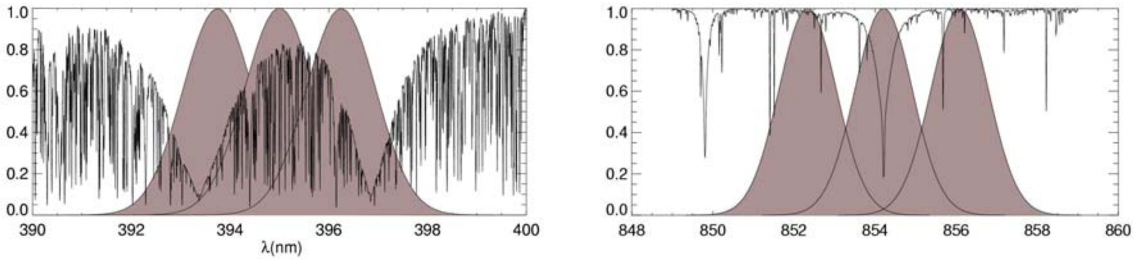

Fig. 1: Fraunhofer lines at 395 nm and 854 nm. Solar irradiances are normalized to one. we added the nominal spectral response functions for the micro channels.

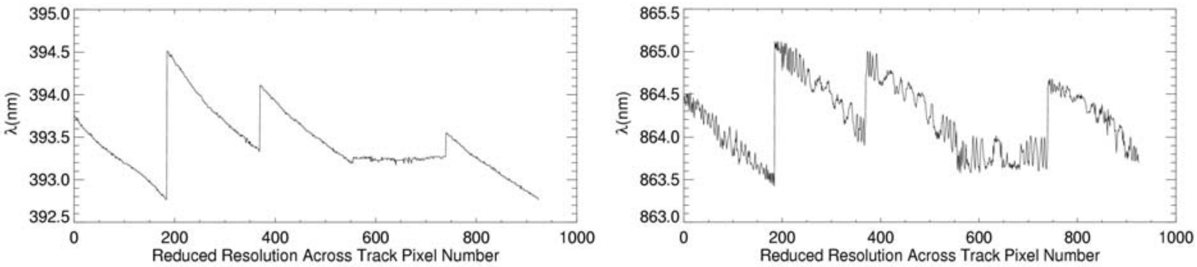

Fig. 2: Results of the Fraunhofer calibration at 395 nm and 854 nm.

Project number	
Project acronym	
Project title	CalVal Support System
Annex No.	4.2.6.2
Title	The in-flight spectral calibration of MERIS using the O2 band A
Version	0.1
Author(s) and affiliation(s)	Steven Delwart, ESTEC, ESA René Preusker, Jurgen Fischer, Freie Universität Berlin Ludovic Bourg, ACRI Richard Santer, ULCO Didier Ramon, HYGEOS
Modification history	17/05/2006
Distribution	Public

Experimental protocol

MERIS is a programmable spectroradiometer. Its fifteen spectral bands are programmable by ground command both in width and in position by steps of 1.25nm.

The specific bands to derive the oxygen transmittance are plotted in Fig. 1. In full line, we reported two adjacent bands to the oxygen absorption region. Also full line, we just remind the nominal MERIS band in the oxygen absorption. This band is not used here. Instead, ten spectral bands, in dashed lines, are used to cover the oxygen absorption region, and two bands are used as reference. By interpolation between these two reference bands to a given oxygen band, it is possible to derive the oxygen transmittance. The three other bands are used to derive a surface type classification using blue, red and near infrared channels.

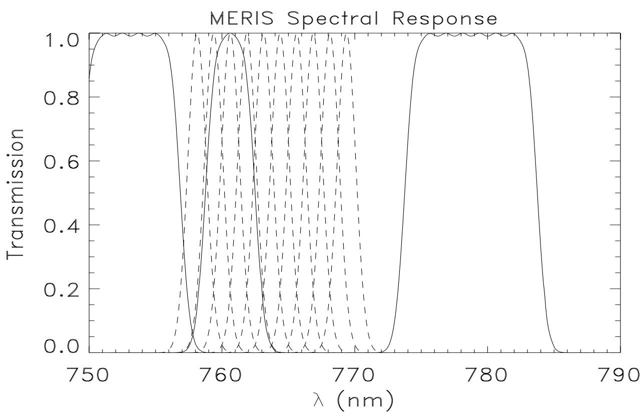

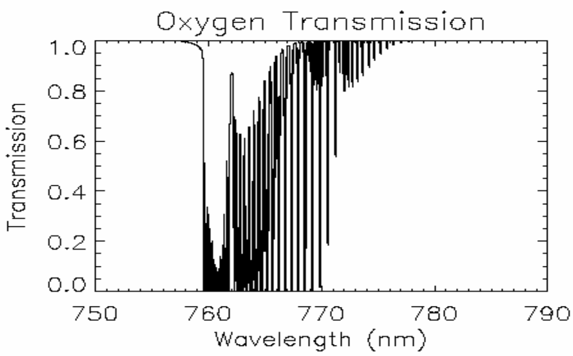

Figure 1:Left: MERIS spectral response and monochromatic atmospheric transmission for the OXYGEN absorption bands region. The dashed lines correspond to the 10 narrow channels within OXYGEN absorption bands used for this in-flight experiment. The full lines correspond to the broad channels of the nominal MERIS band setting.

Right: the oxygen transmission as computed by a line by line code.

The pressure homogenisation algorithm

The method is based on the determination of the surface pressure from the oxygen O2A band (Santer et al., 1999) and is fully described in Dubuisson et al., 2001. In this spectral range (759 to 770 nm), the solar radiation measured at the top of the atmosphere depends strongly on oxygen absorption and therefore on surface elevation. Surface pressure can be estimated from a band ratio R, of measurements made in and close to the oxygen A-band. When the atmospheric scattering cannot be neglected (i.e. in clouds), the retrieved apparent pressure P_{app}, is lower as some measured photons originate from scattering above the ground surface. The ratio R is well correlated to the product mP^2, where m is the air mass, and may be directly converted into a pressure using a polynomial regression

(Fischer and Grassl, 1991; Koelemeijer et al., 2001). In the pressure homogenisation method, we compute one surface pressure for each oxygen narrow O2-x band for a given □ and iterate on the spectral shifts until the difference between the 9 retrieved pressures is minimum.

The algorithm implemented, (see Dubuisson et al, 2003, for more details), is the following:

1. Make sub-scenes of 200 records in the along track direction for each MERIS half-orbit and average the 200 records to produce a unique radiance vector L_j for bands O2-0 to O2-8, and for band Ref-1 L_{ref}. The resulting vectors have the size of the number of across-track pixels in reduced resolution mode.
2. Compute the 9 transmission vectors
3. Start a loop over λ from 759.625 nm in steps of 0.01nm
4. Compute the surface pressure P_j according to equation 3 for each across track sample - 9 pressure vectors.

$$Log_{10}\left(mP_j^{\,2}(\Delta\lambda)\right)=\sum_{i=0}^{4} a_i(\Delta\lambda)\left(L_j/L_{ref}\right)^i \qquad (1)$$

where a_i are the polynomial coefficient of the pressure retrieval, and j the 9 different pressure measurements.

5. Compute a correlation vector from the 9 pressure vectors
6. Loop on λ until the pressure correlation is maximised. This has to be performed independently for all across track elements of the vector
7. Return the spectral shift.

The Look-Up-Table (LUT) of polynomial coefficients a_i has been calculated using the MERIS spectral response, over a spectral range of approximately 2nm (i.e [759.625, 761.615] nm for O2-2) with a step of 0.01nm. The LUT has been computed from a line-by-line code and the HITRAN 2000 spectroscopic database using surface pressures ranging from 1050 to 700 hPa and air masses ranging from 2 to 8.

The Oxygen calibration - The neural network algorithm

A convenient way to describe the gaseous absorption in a scattering atmosphere is the probability density function of the photon geometrical path (PDFGP). The usage of the PDFGP has the advantage that, according to the equivalence theorem (Bakan and Quenzel, 1976; Stephens and Heidinger, 2000), it allows in many cases the de-coupling of scattering and of absorption.

$$I(\lambda_i)=I^*(\lambda)\int_0^\infty PDFGP(l)\exp(-k(\lambda).l)dl \qquad (2)$$

Here $I(\lambda)$ is the monochromatic radiance at the wavelength λ reaching a sensor, k is the volume extinction coefficient and $I^*(\lambda)$ is the radiance in an absorption free atmosphere and l is the photon path length.

The integral on the left side of equation (4) can be approximated using an effective photon path length L and an effective volume extinction coefficient k_{eff} depending on the response function of each MERIS micro band.

$$I(\lambda_i)\approx I_0.\exp\left(-k_{eff}(\lambda_i)L\right) \quad (3)$$

The approximation used to derive equation (3) assumes that L does not depend on λ. This is not strictly true, but the approximation is still valid because k_{eff} varies much more rapidly with λ than L does.

Finally, the gradient

$$G(\lambda_i)=1-\frac{1n\left(I(\lambda_i)\right)-1n(I_0)}{1n(I_{\min})-1n(I_0)}\approx 1-\frac{k_{eff}(\lambda_i)}{k_{eff}(\lambda_{\min})} \qquad (4)$$

where I_{min} , the minimum measured radiance at the centre wavelength λ_{min} is used for normalization. $G(\lambda_I)$ is then independent of the physical properties of the atmosphere and depends primarily on the spectral properties of the radiometer.

In order to make use of the spectral dependence of the measured gradient on the spectral position of the detector element, a neural network has been trained using results of radiative transfer computations using the MOMO code (Fell and Fischer, 2001). This code assumes an isotropic surface reflection and a plane parallel atmosphere, but allows the use of any vertical distribution, scattering particles, optical thickness and spectral resolution to be considered. The surface pressure, the aerosol optical thickness and the albedo of the surface were systematically varied according to table 1.

parameter	Values/range
Surface pressure [hPa]	980,995,1010,1025,1040
Aerosol optical thickness	0.05,0.1,0.15,0.20,0.25
surface albedo	0.0,0.1, ... ,0.9
Total airmass	2-8

Table 1: Parameter used for the NN simulations.

The positions of the 7 bands (O2-0- O2-6) were shifted identically by a step of 0.01 nm values over a range of -1 nm and +1 nm with respect to their nominal positions. The input for the neural network is the normalized spectra $G(\lambda_l)$ and the airmass, and the output is the corresponding spectral shift of the bands (O2-0 - O2-6) for every scan line. The final spectral calibration vector is the median of the scan line results over the scene considered (Complete Orbit, or sub-scene).

For more details see Delwart et al, 2006

References

Bakan S. and Quenzel H., 1976: Path length distribution of photons scattered in turbid atmospheres. *Contribution to Atmospheric Physics*., **46**.

Barnes R. A., and Eplee, Jr. R. E., 1996: The SeaWiFS solar diffuser, In R. A. Barnes, E-n. Yeh, and R. E. Eplee, Jr., eds., SeaWiFS Calibration Topics, Part 1, NASA Tech. Memo. 104566 (NASA Goddard Space Flight Center, Greenbelt, Md.), Vol. **39.**

Dubuisson P., Borde R., Schmechtig C., and Santer R., 2001: Surface pressure estimates from satellite data in the oxygen A-band: Applications to the MOS sensor over land. *Journal of Geophysical Research*, D, **106**, 27277-27286 pp.

Dubuisson P., Borde R., Desailly D., and Santer R., 2003: In flight spectral calibration of the oxygen-A band channel of MERIS. *International Journal of Remote Sens*ing, Vol. **24**, No. 5, p. 1177-1182.

Fell F., and Fischer J., 2001: Numerical simulation of the light field in the atmosphere-ocean system using the matrix-operator method. *Journal of Quantitative Spectroscopy & Radiative Transfer*, **69**, 351-388 pp.

Fischer J., and Grassl H., 1991: Detection of cloud-top height from backscattered radiances within the oxygen A-band. Part. I: theoretical study. *Journal of Applied Meteorology*, **10**,. 1245-1259 pp.

Irvine W. M., 1964: The formation of the absorption bands and the distribution of photon optical paths in a scattering atmosphere. *Bulletin of the Astronomical Institutes of the Netherlands*, **17**.

Koelemeijer R.B.A., Stammes P., Hovenier J.W., and De Haan J.F., 2001: A fast method for retrieval of cloud parameters using oxygen A-band measurements from the Global Ozone Monitoring Experiment., *Journal of Geophysical Research,* D, **106**, 3475-3490 pp.

Santer R., Carrere V., Dubuisson P., and Roger J.C., 1999: Atmospheric correction over land for MERIS. *International Journal of Remote Sens*ing, **20**, 1819-1840 pp.

Stephens, G and A. Heidinger, 2000: Molecular Line Absorption in a scattering atmosphere I; Theory. *Journal of Atmospheric Sciences*, 57.1600-1614Th.

Delwart S., Preusker R., Bourg L., Santer R., Ramon D., Fischer J., 2006. MERIS In-flight Spectral Calibration. Accepted for publication to the International Journal of Remote Sensing.

Project number	
Project acronym	
Project title	CalVal Support System
Annex No.	6.1.a
Title	**S**econd **S**imulation of a **S**atellite **S**ignal in the **S**olar **S**pectrum
Version	1
Author(s) and affiliation(s)	Vermote Eric University of Maryland
Modification history	Received 14 October 2005
Distribution	

6S – **S**econd **S**imulation of a **S**atellite **S**ignal in the **S**olar **S**pectrum – is a basic radiative transfer (RT) code used for calculation of look-up tables in the MODIS atmospheric correction algorithm [Vermote et al., 1997a, 2002]. It enables accurate simulations of satellite and plane observations, accounting for elevated targets, modeling of realistic molecular/aerosol/mixed atmospheres, use of anisotropic and Lambertian surfaces, and calculation of gaseous absorption. It is one of the most widely used and heavily documented RT codes known in the scientific remote-sensing community. The latest updates on the code status (dated May 2005) include a public release of its new vector version, 6SV1, capable of accounting for radiation polarization, which can be downloaded from ftp://kratmos.gsfc.nasa.gov/pub/eric/6S. An inexperienced user is advised to address herself/himself to a special Web interface, available at http://6s.ltdri.org, which can help her/him to learn how to use the code and to build necessary input files.

As its scalar predecessors, 6SV1 is based on the method of successive orders of scattering (SOS) approximations [Deuze et al., 1989; Vermote et al., 1997b]. The effects of polarization are included through the calculation of four components of the Stokes vector, describing the intensity, degree of polarization, plane of polarization and ellipticity of an electromagnetic wavelength [Liou, 1980]. The accuracy of RT calculations can be varied by changing the number of calculation angles and layers. By default, the code uses the "standard accuracy" conditions which provide the user with a relative accuracy of approximately 0.4%.

The code covers a wide range of spectral conditions, from 350 to 3750 nm. The input geometric and spectral options includes not only a user-defined sun-sensor configuration, but also those peculiar to major satellites such as Meteosat, Goes East, Goes West, NOAA PM, NOAA AM, SPOT, and Landsat. Molecular atmosphere modeling incorporates six code-embedded models (tropical, midlatitude summer, midlatitude winter, subarctic summer, subarctic winter, and US Standard 62) and two user-defined models (one with the user-supplied atmospheric parameters and the other with a profile from US 62 and the user-supplied concentrations of water vapor and ozone). Aerosol atmosphere modeling includes six code-embedded aerosol models (continental, maritime, urban, desert, biomass burning and stratospheric), one 4-component model with the user-specified percentage of each component, three statistical distributions with user-defined parameters (multimodal Log Normal (up to 4 modes), modified Gamma, Junge Power-Law), a special option for incorporating AERONET (Aerosol Robotic Network) sun-photometer measurements, and an option to read previously-calculated aerosol parameters from a file. A vertical aerosol profile can be specified arbitrarily by up to 50 layers in the height range from 0 to 100 km. The accuracy of aerosol scattering phase function modeling is controlled through the variation of the number of scattering angles. By default, the code uses an exponential aerosol profile with a height of 2 km and 83 scattering angles. Ground surface modeling includes simulations of homogeneous and non-homogeneous surfaces with/without directional effect. There is also a choice of ten different BRDF (bidirectional reflectance function) models.

6SV1 has been extensively validated against Coulson's tabulated values, which represent the exact solution of the Rayleigh problem with polarization [Coulson et. al., 1960], other RT codes and ocean surface reflectance measurements. The validation against other codes was performed separately in vector and scalar modes for a wide range of atmospheric, spectral and geometrical conditions. In scalar mode, 6SV1 was tested against SHARM [Lyapustin et al., 2002] and DISORT [Stamnes et al., 1988]. In vector mode, 6SV1 was tested against Monte Carlo [Bréon, 1992] simulations. The validation against ocean surface reflectances was performed using MOBY (the Marine Optical Buoy System) data collected near Lanai Island in January-October 2003. MODIS AQUA top-of-atmosphere (TOA) reflectances, measured over Lanai Island, were corrected using 6SV1 and corresponding AERONET measurements and then compared to the MOBY surface reflectances. The obtained results have confirmed good performance of 6SV1. The maximum relative difference between the code outputs did not exceed 0.08% for SHARM and DISORT, 0.21% for Coulson's tabulated values and 0.7% for the Monte Carlo simulations, which is negligible compared to the 2% accuracy of raw MODIS TOA reflectances. Also, the agreement between the corrected AQUA and the MOBY surface reflectances was 0.001 to 0.002 for the 400-550-nm region, satisfying a general requirement of the 10^{-3} accuracy for the retrieval of ocean surface reflectances. The conducted research was summarized in the manuscript Kotchenova et al., submitted for publication in October 2005.

Bréon, F.-M., Reflectance of broken cloud fields: simulation and parameterization, *Journal of the Atmospheric Sciences*, 49, 1221-1232, 1992.

Coulson, K. L., J. V. Dave, and Z. Sekera, Tables related to radiation emerging from a planetary atmosphere with Rayleigh scattering, University of California press, 1960.

Deuze, J. L., Herman, M. and Santer, R. (1989), Fourier series expansion of the transfer equation in the atmosphere-ocean system, J.Q.S.R.T. 41(6):483-494.

Kotchenova, S.Y., E. F. Vermote, F. Klemm and R. Materesse, Validation of a New Vector Version of the 6S Radiative Transfer Code for Atmospheric Correction of MODIS Data (Part I), submitted to Applied Optics in October 2005.

Liou, K.-N., An introduction to atmospheric radiation, Academic Press, Inc., California, 1980.

Lyapustin, A., Radiative transfer code SHARM-3D for radiance simulations over a non-Lambertian non-homogeneous surface: intercomparison study, Applied Optics, 41(27), 5607-5615, 2002.

Stamnes, K., S. C. Tsay, W. Wiscombe, and K. Jayaweera, Numerically stable algorithm for discrete-ordinate method radiative transfer in multiple scattering and emitting layered media, Applied Optics, 27(12), 2502-2509, 1988.

Vermote, E. F., N. Z. El Saleous, C. O. Justice, Y. J. Kaufman, J. Privette, L. Remer, J.-C. Roger, and D. Tanré, Atmospheric correction of visible to middle infrared EOS-MODIS data over land surface, background, operational algorithm and validation, Journal of Geophysical Research, 102 (D14), 17131-17141, 1997a.

Vermote, E. F., D. Tanré, J. L. Deuzé, M. Herman, and J. J. Morcrette, Second Simulation of the Satellite Signal in the Solar Spectrum, 6S: An overview, IEEE Transactions on geoscience and remote sensing, 35(3), 675-686, 1997b.

Vermote, E. F., N. Z. El Saleous, and C. O. Justice, Atmospheric correction of MODIS data in the visible to middle infrared: first results, Remote Sensing of Environment, 83, 97-111, 2002.

Project number	
Project acronym	
Project title	CalVal Support System
Annex No.	6.1.b:
Title	RTC for calibration in the solar domain; the Successive Order of Scattering code.
Version	1
Author(s) and affiliation(s)	R. Santer, ULCO
Modification history	
Distribution	

Inherent optical properties

Application of the Rayleigh theory to the atmosphere results on the choice of the pressure-temperature profile (here the mid-latitude summer) and on the molecular anisotropy (δ = 0.0279).

The *Mie* theory gives the inherent optical properties (*i.e.*, extinction and scattering coefficients and phase function) of a spherical particle characterized by its complex refractive index m and its geometrical radius r. A given medium can be described by an unique particle mode with associated refractive index m and a size distribution n(r) or by multimode distributions.

The radiative transfer equation

The RTCs simulate the radiance field at TOA in the visible (VIS) and near infrared (NIR) regions, taking into account, in the one hand, the inherent optical properties and the concentrations of the atmospheric constituents, and in the other hand, the lightening and viewing geometrical conditions.

Considering an isotropic medium illuminated by an unpolarized radiation beam, i.e., with the *Stokes* parameters $(E_o,0,0,0)$ and with symmetrical boundary conditions with respect to the incident plane, the *Stokes* vector components can then be developed in azimuth using a *Fourier* series expansion (Lenoble, 1985). By expanding the scattering phase matrix in the same way, the RTE splits up into a set of independent equations with μ as the unique angular coordinate:

$$\mu \,.\, \frac{dL_m(\delta;\mu)}{d\delta} = L_m(\delta;\mu) - \frac{\omega_o(\delta)}{4\pi} \,.\, \tilde{M}_m(\delta;\mu,\mu_o) \,.\, E_o \,.\, e^{-\delta/\mu_o} - \frac{\omega_o(\delta)}{2} \,.\, \int_{-1}^{1} \tilde{M}_m(\delta;\mu,\mu') \,.\, L_m(\delta;\mu') \,.\, d\mu' \qquad (1)$$

where the prime notation denotes the incident field light, (μ_o,φ_o) the solar zenithal and azimuthal angles, ω_o and $\tilde{M}$ respectively the single scattering albedo and the scattering phase matrix located at δ within the elementary layer.

The number of independent equations depends on the length of the scattering phase function development (*i.e.*, the number of terms used in the *Legendre* polynomial expansion). Each equation can then be solved independently in the *Fourier* space before being recombined to yield to the solution in the *Euclidian* space.

The RTC / SO (Deuzé et al., 1989) solves the RTE for a purely scattering atmosphere over a *Lambertian* ground reflector with clear-sky conditions. Radiances are then computed for each term m of the *Fourier* series. Scattering phase function of the aerosols are approximated by L=80 terms in the *Legendre* expansion.

The upwelling $L_m^{\uparrow(1)}$ and downwelling $L_m^{\downarrow(1)}$ radiances arising from primary scattering $(n=1)$ are computed for each term m of the *Fourier* series, up to m=L, as follows:

$$\begin{cases} L_m^{\uparrow(1)}(\delta,\mu>0)=\dfrac{\omega_o}{4\pi\mu}.\,\tilde{E}_s\,.\displaystyle\int_{\tau_1}^{\tau} e^{\delta'/\mu_o}\,.\,e^{-(\delta'-\delta)/\mu}\,.\,\tilde{M}_m(\delta',\mu,\mu_o)\,.\,d\delta' \\ L_m^{\downarrow(1)}(\delta,\mu>0)=\dfrac{\omega_o}{4\pi\mu}.\,\tilde{E}_s\,.\displaystyle\int_{0}^{\tau} e^{\delta'/\mu_o}\,.\,e^{-(\delta-\delta')/\mu}\,.\,\tilde{M}_m(\delta',-\mu,\mu_o)\,.\,d\delta' \end{cases} \qquad (2)$$

The *Stokes* vector $\tilde{E}_s=(E_o,0,0,0)$ of the incident solar beam is unpolarized and E_o represents the extraterrestrial solar irradiance.

For the multiple scattering $(n>1)$, the upwelling $L_m^{\uparrow(n)}$ and downwelling $L_m^{\downarrow(n)}$ radiances at the order n provide from the signal contributions at the order $(n-1)$. Thus for a given order n the signal is integrated over μ' and δ as follows:

$$\begin{cases} L_m^{\uparrow(n)}(\delta,\mu>0)=\dfrac{\omega_o}{2\mu}.\displaystyle\int_{\tau_1}^{\tau} e^{-(\delta'-\delta)/\mu}.\left[\int_{-1}^{1}\tilde{M}_m(\delta',\mu,\mu')\,.\,L_m^{(n-1)}(\delta',\mu')\,.\,d\mu'\right].\,d\delta' \\ L_m^{\downarrow(n)}(\delta,\mu>0)=\dfrac{\omega_o}{2\mu}.\displaystyle\int_{0}^{\tau} e^{-(\delta-\delta')/\mu}.\left[\int_{-1}^{1}\tilde{M}_m(\delta',-\mu,\mu')\,.\,L_m^{(n-1)}(\delta',\mu')\,.\,d\mu'\right].\,d\delta' \end{cases} \qquad (2)$$

Integration with respect to μ' is performed using a *Gaussian* quadrature with 48 angles and the computation with respect to δ is accomplished by dividing the atmosphere into 33 layers. Due to the fact that aerosols and molecules present different vertical distributions, this atmosphere is then built using aerosol optical depth profile and *Rayleigh* optical depth (with a scale height of 8km) selected by the operator. Mixing rates (defined as the ratio of the scattering coefficient of an atmospheric component to the sum on the extinction coefficients of all the atmospheric components) of aerosol and molecular optical properties are determined for each atmospheric layer.

For a given term m of the *Fourier* series, the iterative process over the SO of scattering $(n>1)$ is broken as soon as the SO of scattering converge into a geometrical series. If this is the case, the iterations are then stopped and the tail of the geometrical series is added to the contribution of the scattering order for which the convergence was detected. Generally, this test is carried out firs and greatly reduces the computational time

The accuracy of the SO code is linked to the discretization in sublayers used in Eq. (2) and also in the Gaussian integration of Eq. (3).

Exemple of input-output

Paramètres de simulation : Description des entrées – sorties, paramètres physiques et options de traitements		**SOS.ksh**
Répertoires de la base des fichiers de réflexion de surface et des fichiers de Mie		
repMIE	Répertoire de stockage des fichiers de Mie	
Nom des fichiers Trace des programmes		*Saisir 0 pour ne pas générer de fichier Trace*
Nom par défaut des fichiers de profil et d'aérosols (fichiers écrasés à chaque simulation)		
ficDefautProfil	Nom par défaut du fichier PROFIL	*Utilisé en absence de fichier Utilisateur*
ficDefautAer	Nom par défaut du fichier AEROSOLS	
CONDITIONS DE SURFACE		
typeSurf	Numéro de type de surface 0 : surface lambertienne d'albédo rho	
rho	Albédo de surface (voir tableau 1)	
CONDITIONS ATMOSPHERIQUES		
Profil atmosphérique		
ficPROFIL	- DEFAULT pour que le code utilise le nom par défaut ficDefautProfil. Le logiciel utilise alors les paramètres suivants.	
Molécules		
Ron= 0.9587	Facteur de dépolarisation moléculaire	
tauRay	Epaisseur optique Rayleigh (voir tableau 1)	
HR=8	Echelle de hauteur du profil moléculaire (km)	
Aérosols : profil		
tauAer	Epaisseur optique des aérosols (non tronquée) (voir tableaux 2 et 3)	
HA=2	Echelle de hauteur du profil d'aérosols (km)	
Type de profil		
profil	Type de profil simulé : 1 : profil défini par simples échelles de hauteur	
Propriétés radiatives des aérosols		
ficAERgranu	Nom du fichier Aérosols - DEFAULT pour que le code utilise le nom par défaut ficDefautAer. Le logiciel utilise alors les paramètres suivants.	
wa	Longueur d'onde (en µm) : .38, .44, .55, .87	
tronca	Indice de troncature 0 : pas de troncature	
Aérosols : granulométrie		
modalite	Modalité de la granulométrie 0 : modèle mono-modal	
Si modalite = 0 : paramètres de Mie (granulométrie mono-modale)		
Mr=1.44	Partie réelle de l'indice de réfraction	
Mi=0	Partie imaginaire de l'indice de réfraction (valeur négative)	
alphaMin=0	Valeur minimale du paramètre de taille	
alphaMax=200	Valeur maximale du paramètre de taille	
nomFicMIE	Nom du fichier de Mie qui sera stocké sous repMIE : MIE144	
CONDITIONS D'ECLAIREMENT		
tetas	angle zénithal solaire en degrés (0 < tetas < 90°) Utilisé seulement si imus < 0 (voir liste des cosinus de 10 angles à convertir en deg. + 3 angles)	

CHOIX DU TYPE DE SORTIE		
niveau	Niveau du profil	-1 : sortie standard (L↑ TOA, L↓ sol) n : luminance montante et descendante au niveau n du profil ($0 \leq n \leq$ SOS_OS_NT)
Igmax=50	Ordre maximal de diffusion	
Ipolar=1	Indice de coupure de la polarisation	0 : simulation des OS sans polarisation 1 : simulation normale avec polarisation
optionVisee	Indice de type de sortie	1 : plan de visée
Phi=0	Azimut relatif (en degrés) Utilisé si optionVisee = 1	
NOM DES FICHIERS RESULTATS DES OS		
ficOSbin	Nom du fichier binaire résultat des OS en décomposition en séries de Fourier	
ficOSup	Nom du fichier ascii résultat pour le champ montant	
ficOSdown	Nom du fichier ascii résultat pour le champ descendant : exp : 380_30_05 Lambda=380 Tetas=30 Taua=0.05	

Tableau 4: Paramètres de simulations contenus dans le fichier SOS.ksh

References

Deuzé J.L., Herman M., Santer R., 1989 ; Fourier series expansion of the transfer equation in the atmosphere-ocean system. *Journal of Quantitative Spectroscopy and Radiatitive. Transfer , **41**(6) :483-494.*

Herman M and J.L. Deuzé, «Observation de la terre en lumière polarisée. Simulations numériques par le code des ordres successifs de diffusion. « Notice scientifique», Laboratoire d'Optique Atmosphérique, Lille, 2002.

Project number	
Project acronym	
Project title	CalVal Support System
Annex No.	6.2.3
Title	Measurements for calibration in the solar domain: The automatic CIMEL radiometer
Version	1.0
Author(s) and affiliation(s)	Santer R.
Modification history	First draft: 01/09/2005
Distribution	public

Objectives of the measurements

One unique instrument has been designed to characterize both the surface and the atmosphere in order to predict the TOA radiance.

The heritage

The Cimel CE 318N, see figure 1, is an automatic ground based radiometer devoted to the characterization of the aerosols. The optical part is composed by a filter wheel and two collimators (« SUN » et « SKY ») of respectively 1° and 3° field of view associated to two silicium detectors. The "SUN" collimator is used for direct solar irradiance measurements while the « SKY » collimator is used for sky radiance measurements.

AERONET is a network of Cimel instruments (***http://aeronet.gsfc.nasa.gov).l***

Figure 1: the CIMEL radiometer

The scanning protocol is described in figure 2. Mode (a) gives extinction measurements while sky radiances are collected both in the principal plane and in the amulcantar.

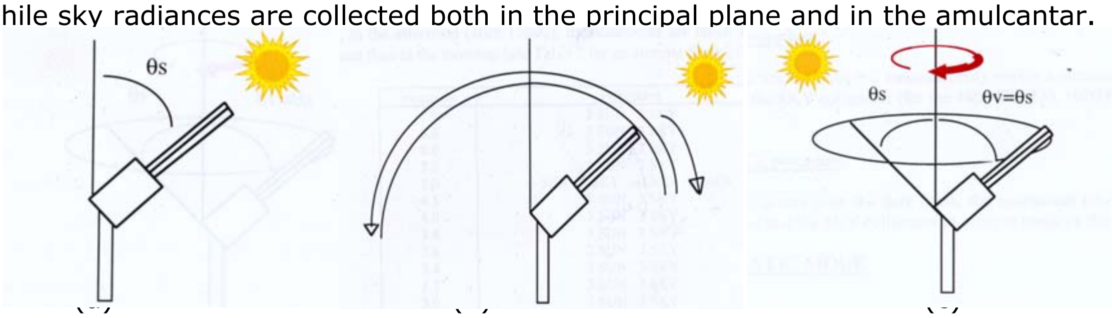

Figure 2: The scanning modes: (a) sun, (b) principal plane, (c) almulcantar.

The CIMEL La Crau instrument

Basic concept

Compared to the Cimel CE 318N, this new instrument has two collimators, both of 3° field of view. One is associated to a silicium detector while the second is associated to a germanium detector in order to extend the spectral domain to the middle infra red.

Spectral configuration

Three filters, 550nm, 670nm, 870nm, 10nm wide, have been chosen to correspond to the SPOT-HRV bands. We also choose two filters, 440nm (10nm wide) and 1600nm (50nm wide) to correspond to VEGETATION bands. Two others filters (10nm wide) have been added to describe as much as possible atmosphere components, the first one 937nm is dedicated to water vapour study and the second one, 1020nm[4]. Finally, a filter at 380 nm (10nm wide) has been introduced to the absolute calibration of the station with reference to the Rayleigh scattering.

Scanning mode

As soon as the air mass reaches m=5, then the scanning protocol, illustrated in figure 2, begins:

(a) Atmosphere characterisation

- Searching the sun position as a function of the hour.

-3 measurements of the optical depth for every filter.

-Almucantar measurements ($\theta v=\theta s$, $\Delta\varphi$ varies from 0 to 360°) for 4 filters: 380nm, 550nm, 870nm, 1600nm

-Principal plane measurements for 6 filters: 380nm, 440nm, 550nm, 670nm, 870nm, 1600nm

(b) Ground characterisation. Ground mode is similar to figure 2(c) but with down looking view as illustrated in figure 3.

- Pointing to the South

-For a view angle, facing the ground, from 5 to 60 degrees by step of 5 degrees

-For each of five filters: 440, 550, 670, 870, 1600

-Ground measurements on 360 degrees with an azimutal steps of 5 degrees

This complete protocol takes one hour and 6 minutes, the (a)+(b) sequences continue until the air mass has over passed 5 in the afternoon.

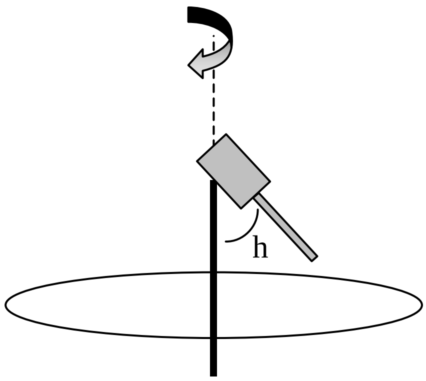

Figure 3: The scanning modes for the surface reflectance measurements

Implementation

Figure 4: left: Implementation of the instrument on the La Crau site on a 10 meter height pole. Solar panel is used for power supply. Data transmission is realized with a cellular phone.

Figure 5: below: Surface reflectance at 670 nm as measured by the CIML instrument. The shade of the pole can be seen bottom left. Bidirectional effects are illustred by the left/right dysymetry.

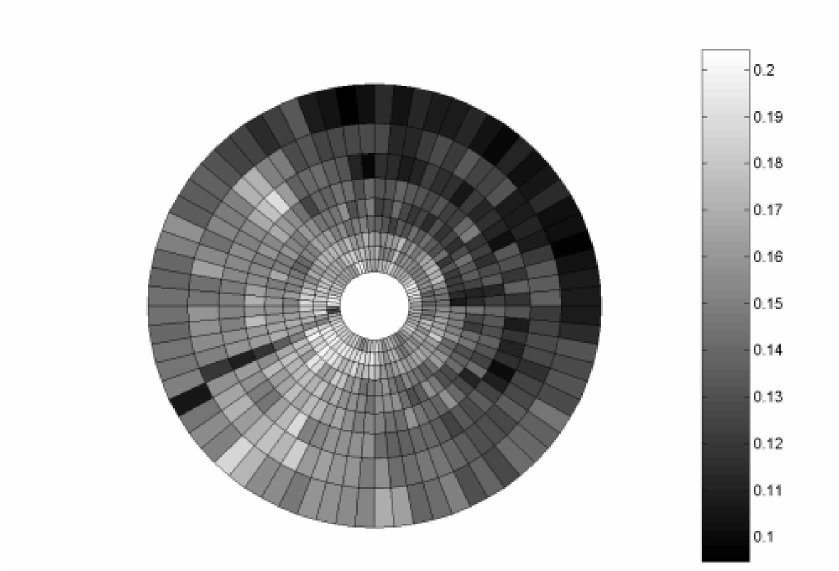

References

SANTER R., ROGER J.C., SCHMECHTIG C., MEYGRET A. (1997). An automatic radiometer ground-based station for vicarious calibration. The European Symposium on Aerospace Remote Sensing, London, UK, 22-26 Sept,

SANTER R. SIX C., BUIS J. P., (2002). Vicarious calibration on land site using automatic ground basedoptical measurements. Applications to SPOT HRV. Proceedings of SPIE Volume: 4891, p524-534 . Optical Remote Sensing of the Atmosphere and Clouds III . Editor(s): Hung-Lung Huang, Daren Lu, Yasuhiro Sasano.

Project number	
Project acronym	
Project title	CalVal Support System
Annex No.	6.2.4
Title	The SeaPRISM CIMEL radiometer
Version	1
Author(s) and affiliation(s)	Giuseppe Zibordi, Jean-François Berthon and Frédéric Mélin Joint Research Centre, Ispra
Modification history	
Distribution	

The CE-318 radiometer manufactured by CIMEL (France, Paris) for the characterization of the aerosol optical properties, has also been shown capable of performing measurements suitable for the determination of the water leaving radiance (Zibordi et al. 2004). These measurements include sky and sea radiance observations made in daylight conditions every 30 minutes at 7 center-wavelengths λ (i.e., 412, 440, 500, 555, 670, 870, and 1020 nm) chosen to support both atmospheric and marine applications (see Fig.1). The specific CE-318 radiometer allowing for the execution of above water radiometric measurements is called SeaWiFS Photometer Revision for Incident Surface Measurements (SeaPRISM). The system supports data transmission through satellite link and provides the capability of programming some of the parameters defining the measurement protocol (i.e., the viewing angle θ and the relative azimuth with respect to the sun φ, the gain for each channel, and, the numbers N_T and N_i of above-water and sky measurements, respectively).

Figure 1. Picture of the SeaPRISM system.

The measurement sequence develops through successive steps:

1. A series of direct sun measurements acquired at all channels for the determination of the direct sun irradiance $E(\phi_0, \theta_0, \lambda)$ with ϕ_0 and θ_0 sun azimuth and zenith, respectively ;
2. A sequential set of N_T radiance measurements for determining $L_T(\varphi, \theta, \lambda)$, N_i sky radiance measurements for determining $L_i(\varphi, \theta', \lambda)$, and one dark measurement for the channel corresponding to the center wavelength λ;

3. Step 2 is sequentially repeated for each channel included in the sea-viewing scenario.

If the sun is cloud covered, which is detectable through step 1, the measurement sequence is cancelled. For clear-sky conditions, the $E(\phi_0, \theta_0, \lambda)$ data allow for the determination of the aerosol optical thickness, $\tau_A(\lambda)$, which is needed for computing the normalized water-leaving radiance $L_{WN}^{SP}(\lambda)$.

The viewing geometry for the SeaPRISM systems operated on the Acqua Alta Oceanographic Tower (AAOT) is defined by θ=40° (with $\theta'=\pi-\theta$) and φ=90°, respectively. In addition, N_i=3 and N_T=11 are chosen, so the execution of a complete measurement sequence of sky and sea measurements takes approximately 6 minutes.

The determination of the water leaving radiance $L_W^{SP}(\varphi,\theta,\lambda)$ from SeaPRISM measurements is made in agreement with Hooker et al. (2004) and Zibordi et al. (2004) with

$$L_W^{SP}(\varphi,\theta,\lambda) = L_T(\varphi,\theta,\lambda) - \rho(\varphi,\theta,\theta_0,W) L_i(\varphi,\theta',\lambda)\,, \tag{1}$$

where $L_T(\varphi,\theta,\lambda)$ results from averaging of the 20% of the N_T observations exhibiting the lowest radiance values, $L_i(\varphi,\theta',\lambda)$ results from averaging of the N_i observations, and $\rho(\varphi,\theta,\theta_0,W)$ is the sea surface reflectance, mostly a function of the measurement geometry (identified by φ, θ, θ_0) and wind speed W. The surface reflectance, $\rho(\varphi,\theta,\theta_0,W)$ at a given θ and φ, is determined as a function of θ_0 and W using the theoretical results of a study on above-water measurements (Mobley 1999). Given that the radiance field emerging from the ocean is not isotropic (Morel and Gentili 1996), the computation of a nadir-transformed water-leaving radiance, $L_W^{SP}(\lambda)$, from $L_W^{SP}(\varphi,\theta,\lambda)$ is made using

$$L_W^{SP}(\lambda) = L_W^{SP}(\varphi,\theta,\lambda) C_{\Re Q}(\lambda,\theta,\varphi,\theta_0,\tau_a,Chla,W)\,, \tag{2}$$

where the correction term $C_{\Re Q}(\lambda,\theta,\varphi,\theta_0,\tau_a,Chla,W)$ removes the dependence associated with the viewing geometry during data acquisition (Morel et al. 2002) and is given by

$$C_{\Re Q}(\lambda,\theta,\varphi,\theta_0,\tau_a,Chla,W) = \frac{\Re_0}{\Re(\theta,W)} \frac{Q(\lambda,\theta,\varphi,\theta_0,\tau_a,Chla)}{Q_n(\lambda,\theta_0,\tau_a,Chla)}\ . \tag{3}$$

The quantities $\Re(\theta,W)$ and $\Re_0$ (i.e., $\Re(\theta,W)$ at $\theta=0$) account for surface reflectance and refraction, and primarily depend on θ and W. The quantities $Q(\lambda,\theta,\varphi,\theta_0,\tau_a,Chla)$ and $Q_n(\lambda,\theta_0,\tau_a,Chla)$ are the so-called Q-factors at viewing angle θ and at nadir (i.e., $\theta=0$), respectively. The Q-factor mostly depends on φ, θ, θ_0, τ_a, and chlorophyll *a* concentration *Chla* (used here to express the dependence on the seawater inherent optical properties), and describes the anisotropic distribution of the in-water radiance field.

The determinations of the $\Re(\theta,W)$ and $Q(\lambda,\theta,\varphi,\theta_0,\tau_a,Chla)$ terms in (3) are made using look-up tables (Morel et al., 2002) produced for a clear sky with aerosol optical thickness τ_A=0.2 at 550 nm, for various θ_0, θ, φ, *Chla*, and λ. The value of *Chla* is estimated through an iterative process.

The computation of the normalized water leaving radiance $L_{WN}^{SP}(\lambda)$ is made using

$$L_{WN}^{SP}(\lambda) = L_W^{SP}(\lambda) C_{f/Q}(\lambda,\theta_0,\tau_A,Chla)\left(D^2 t_d(\lambda)\cos\theta_0\right)^{-1}, \tag{4}$$

where the correction term $C_{f/Q}(\lambda,\theta_0,\tau_A,Chl)$ accounts for the bidirectional effects, and is defined by

$$C_{f/Q}(\lambda,\theta_0,\tau_A,Chla)=\frac{f_0(\lambda,\tau_A,Chla)}{Q_0(\lambda,\tau_A,Chla)}\left(\frac{f(\lambda,\theta_0,\tau_A,Chla)}{Q_n(\lambda,\theta_0,\tau_A,Chla)}\right)^{-1}, \quad (5)$$

where $f(\lambda,\theta_0,\tau_A,Chla)$ is a function relating the apparent optical properties (and specifically the irradiance reflectance) to the inherent optical properties (Morel et al., 2002). The quantity $f(\lambda,\theta_0,\tau_A,Chla)$ is mostly a function of λ, θ_0, τ_A, and *Chla* (where *Chla* still expresses the dependence on the inherent optical properties). The quantities $f_0(\lambda,\tau_A,Chla)$ and $Q_0(\lambda,\tau_A,Chla)$ are the $f(\lambda,\theta_0,\tau_A,Chla)$ and $Q_n(\lambda,\theta_0,\tau_A,Chla)$ values defined for $\theta_0=0$. The ratios $f_0(\lambda,\tau_A,Chla)/Q_0(\lambda,\tau_A,Chla)$ and $f(\lambda,\theta_0,\tau_A,Chla)/Q_n(\lambda,\theta_0,\tau_A,Chla)$ are also obtained from look-up tables (Morel et al. 2002). The term D^2 in (4) accounts for the variations in the Sun-Earth distance as a function of the day of the year, while the quantity $t_d(\lambda)$ is the atmospheric diffuse transmittance.

Application of SeaPRISM data for ocean color data validation is given in Zibordi et al. (2004) and in Zibordi et al. (2005).

References

S.B. Hooker, Zibordi G., Berthon J.-F. and Brown J.W., "Above-Water Radiometry in shallow coastal waters, " *Appl. Opt.*, vol. 21, pp. 4254-4268, 2004.

C. Mobley, "Estimation of the remote-sensing reflectance from above surface measurements," *Appl. Opt.*, vol. 38, pp. 7442–7455, 1999.

A. Morel, and B. Gentili, "Diffuse reflectance of oceanic waters, III. Implication of bidirectionality for the remote sensing problem," *Appl. Opt.*, 35, pp. 4850–4862, 1996.

A. Morel, Antoine D. and Gentili B., "Bidirectional reflectance of oceanic waters: accounting for Raman emission and varying particle scattering phase function," *Appl. Opt.*, vol. 41, pp. 6289-6306, 2002.

G. Zibordi, Mélin F., Hooker S. B., D'Alimonte D. and Holben B., "An autonomous above-water system for the validation of ocean color radiance data," *IEEE Trans. Geoscience and Rem. Sens.*, vol. 42, pp. 401-415, 2004.

G.Zibordi, Mélin F. and Berthon J.-F., "A time-series of above-water radiometric measurements for coastal water monitoring and remote sensing product validation," *IEEE Geoscience and Rem. Sens. Lett.*, doi: 10.1109/LGRS.2005.858486, 2005.